Study on the Abrasive Retention Capacity on the Surface of Electroplated Diamond Wire Saw

Jintao Zheng
Shandong University
Qian Xie
Shandong University
Peiqi Ge (pqge@sdu.edu.cn)
Shandong University
Jianfeng Meng
Shandong University
Wenbo Bi
Shandong University

Research Article

Keywords: Electroplated diamond wire saw, Abrasive retention capacity, Wire saw slicing, Abrasive sheddin

Posted Date: March 24th, 2021

DOI: https://doi.org/10.21203/rs.3.rs-347682/v1

Study on the abrasive retention capacity on the surface of electroplated diamond wire saw

Jintao Zheng [a], Qian Xie [a], Peiqi Ge [a, b] *, Jianfeng Meng [a, b], Wenbo Bi [a, b]

[a] *School of Mechanical Engineering, Shandong University, Jinan, 250061, China*

[b] *Key Laboratory of High-Efficiency and Clean Mechanical Manufacture at Shandong University, Ministry of Education, Jinan, 250061, China*

*Corresponding author. *Tel./Fax.*: +86 531 88399277. *Email address*: pqge@sdu.edu.cn (Peiqi.Ge).

Abstract

The quality and efficiency of slicing will be reduced if the abrasives on the surface of diamond wire saw shed in sawing. Generally, the diamond abrasives are held on the surface of electroplated diamond wire saw by a nickel-plated layer, and the abrasive retention state, reflecting abrasive shedding, can be characterized by the plastic deformation of the plating layer at the interface between the nickel-plated layer and the abrasive. To gain an in-depth understanding of the abrasive shedding mechanism, a finite element model of the double-cone diamond abrasive embedded in a nickel-plated layer was established in this paper to research the effects of the residual compressive stress and hardness of the nickel-plated layer as well as the protrusion height of the diamond abrasive on the abrasive retention capacity. The results show that the presence of the residual compressive stress in the nickel-plated layer resulted in the decrease of the abrasive retention capacity. And the higher hardness of the nickel-plated layer could enhance its abrasive retention capacity. Furthermore, the depth of the diamond abrasive inside the nickel-plated layer was decreased with the increase of its protrusion height, which would reduce the abrasive retention capacity. Based on the results of the finite element analysis, a calculation procedure of abrasive shedding rate was presented. Subsequently, the slicing experiment of a single crystal silicon rod was carried out by the Meyer Burger RTD6800 multi-wire sawing machine and the electroplated diamond wire saw with a core wire diameter of 65μm. The abrasive shedding rate of the diamond wire saw caused by sawing was analyzed theoretically and experimentally. The research work is of great significance to improve the quality detection and evaluation of electroplated diamond wire saw.

Keywords: Electroplated diamond wire saw; Abrasive retention capacity; Wire saw slicing;

Abrasive shedding

1. Introduction

Electroplated diamond wire saw is widely employed for the sawing of brittle materials due to its high sawing efficiency, low environmental pollution, and low production and manufacture costs [1-3]. With the development of photovoltaic silicon slicing technology, there are higher and higher requirements for the performance of diamond wire saw [4]. Generally, in the production process of electroplated diamond wire saw, the diamond abrasives are deposited on the surface of metal wire by composite electroplating [5], and then attached by a nickel-plated layer. Therefore, the mechanical properties of the nickel-plated layer have a significant effect on the abrasive retention capacity on the surface of the diamond wire saw which is the ability of the nickel-plated layer to bond the diamond abrasive and prevent it from shedding. In the sawing process of crystal material with the diamond wire saw, the removal of the workpiece material is achieved by the scratching of the diamond abrasive. The abrasive shedding caused by sawing force will reduce the quality and efficiency of slicing, and even lead to the wear failure of the diamond wire saw. Therefore, the abrasive retention capacity on the surface of the electroplated diamond wire saw is a key factor that affects its working performance.

Generally, the abrasive retention capacity of nickel mainly depends on the chemical and mechanical action of the interface between them. The former makes the diamond abrasive adhered by the chemical bond formed between diamond abrasive and nickel [6, 7], while the latter prevents the diamond abrasive from shedding by the mechanical occlusion [8]. For the electroplated diamond wire saw shown in Fig.1, the attachment of the diamond abrasives mainly depends on the occlusion effect of the nickel-plated layer. Therefore, the mechanical binding force plays a more important role for the nickel-plated layer to hold the diamond abrasives, which is the focus of this paper.

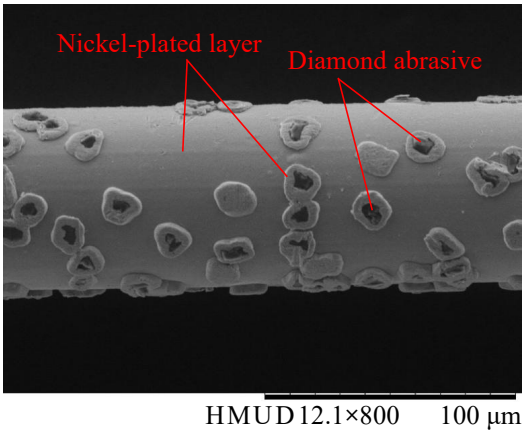

Fig.1 Morphology of electroplated diamond wire saw

The quantitative characterization methods of the abrasive retention capacity mainly include analysis on bending strength, calculation by elasticity equation, and so on [9]. However, in order to improve the sawing ability of diamond wire saw, only the characterization of the abrasive retention capacity can not meet the needs of engineering, so it is necessary to study the mechanism of diamond abrasive shedding. Webb [10] proposed the diamond abrasive retention R, which reflects the relationship between the forces of diamond abrasives participating in sawing. The research shows that only when the R value is greater than 1, the diamond abrasive can be well held on the metal substrate. Xu et al. [11] believed that the abrasive shedding was caused by the interface debonding between the diamond abrasive and the metal-plated layer. When the interface separation gap reaches a certain degree, the abrasive will shed. Besides that, it has been observed that the shapes and orientations of diamond abrasives and the interfacial properties have a significant influence on the abrasive retention capacity. Romanski [8] reported that the abrasive shedding was caused by the deformation of the metal-plated layer embedded with the diamond abrasive. As shown in Fig.2, one side of the plating layer embedded with the diamond abrasive will be squeezed by the loaded abrasive. And when the deformation of the plating layer reaches a certain value, there will be a large gap between the plating layer and the diamond abrasive, which makes the abrasive shed. According to Romanski's research, Konstanty et al. [12] analyzed the influence of the different loading methods for diamond abrasive and the types of the plating layer materials on the diamond abrasive shedding and considered that if the deformation of plating layer reaches 4%-8%, the diamond abrasive will be in the critical shedding state.

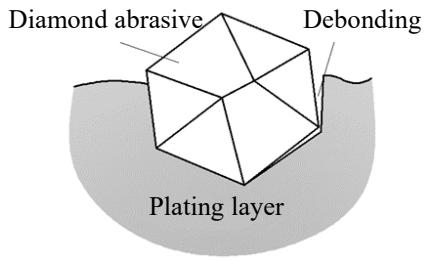

Fig.2 Schematic diagram of diamond abrasive shedding

Up to now, the previous research works mainly focus on the evaluation of the abrasive retention capacity, but the study on the influences of the properties of the plating layer material embedded with the diamond abrasive on the abrasive retention capacity is relatively insufficient. Therefore, aiming at the abrasive retention capacity of electroplated diamond wire saw, the analysis model of the double-cone diamond abrasive embedded in the nickel-plated layer was established by the finite element method in this paper. The influences of the residual stress and hardness of the nickel-plated layer and the protrusion height of the diamond abrasive on the abrasive retention capacity were analyzed by applying sawing force to the abrasive and taking the deformation of the nickel-plated layer as the critical condition to judge the diamond abrasive shedding state. Moreover, based on the results of finite element analysis, a simulation procedure for calculating the abrasive shedding rate was presented. According to the sawing experiment, the theoretical abrasive shedding rate on the surface of electroplated diamond wire saw was compared with the reality, which verified the reliability of the finite element analysis. This research will provide some guidance for the manufacture of electroplated diamond wire saw.

2. Mechanical properties test of nickel-plated layer

2.1 Sample preparation

The abrasive retention capacity of electroplated diamond wire saw is significantly related to the mechanical properties of the nickel-plated layer on its surface, including residual stress and hardness. Since the electroplated diamond wire saw is ultra-fine, it is difficult to directly measure the mechanical properties of the nickel-plated layer. Additionally, the mechanical properties are associated with the internal grain size of the nickel-plated layer which is mainly affected by the material properties and surface state of the substrate at the

beginning of the formation of the nickel-plated layer rather than its shape and structure. Therefore, a T9A steel plate with similar chemical composition and mechanical properties to the core wire of electroplated diamond wire saw is selected as the substrate to prepare the nickel-plated layer sample without diamond abrasive. The electroplated specimen with dimensions of 100×60×40mm is obtained. The structure of electroplating experiment equipment is shown in Fig.3.

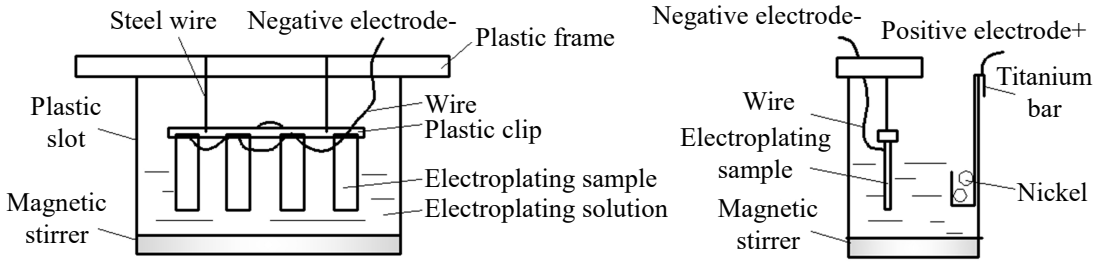

Fig.3 Structure of electroplating experiment equipment

In order to make the mechanical properties of the nickel-plated layer of the specimen consistent with those on the surface of the actual electroplated diamond wire saw, the process of electroplating is set as follows: removing oil by alkali washing, activating by acid washing, plating A layer, plating B layer, and plating C layer. The nickel-plated layers A, B, and C correspond to pre-plating, sanding, and thickening in the production process of electroplated diamond wire saw, respectively. According to the actual production process parameters of the electroplated diamond wire saw with a core wire diameter of 65μm in industry, the main parameters of electroplating experimental are set as shown in Table 1. In the experiment, the constant temperature of electroplating solution is controlled at 50℃, and the nickel-plated layers A, B and C with the thickness of 0.1μm, 1.5μm and 1.6μm respectively are obtained.

Table 1 Main process parameters of electroplating experiment

Process	PH Value	Cathode current density (A/dm²)	Electroplating time (s)
A	3.8	7.9	4
B	4.8	27.3	18
C	3.8	27.3	18

2.2 Measurement of residual stress in nickel-plated layer

The residual stress in the nickel-plated layer is measured by the X\'PERT Pro MPD X-ray instrument in Holland. Because the residual stress in the material is associated with the

change of crystal plane spacing, the lattice strain caused by the stress is consistent with the macroscopic strain calculated according to the elastic theory under a certain stress state [13]

$$\varepsilon_{\varphi\psi} = \frac{1}{2} S_2^{hkl} \sigma_\varphi \sin^2 \psi + \sum \sigma_{ij} S_1^{hkl} \quad (1)$$

Where $1/2S_2^{hkl}$, S_1^{hkl} are X-ray elastic constants; (φ, ψ) is the azimuth of the measuring direction in the sample coordinate system; σ_φ, $\varepsilon_{\varphi\psi}$ are the lattice stress and strain in the measuring direction, respectively; σ_{ij} is the component related to stress. In the measurement process, the lattice strain is expressed by the slip distance of the crystal plane D_{spacing}. When D_{spacing}~$\sin^2\psi$ is linear, the stress value can be obtained by the slope of the straight line, and a positive slope indicates compressive stress whereas a negative slope indicates tensile stress. In this paper, the relationship between D_{spacing} and $\sin^2\psi$ of the sample is shown in Fig.4. The measured results are fitted by the linear fitting method, and it is obtained that the residual compressive stress is 601.6MPa.

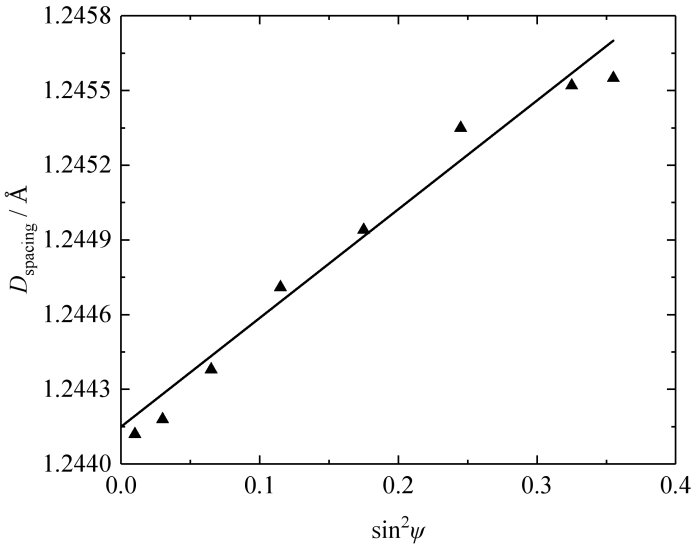

Fig.4 X-ray test result of residual stress in nickel-plated layer

2.3 Measurement of hardness of nickel-plated layer

The hardness and elastic modulus of the nickel-plated layer are measured by the Fischer's HM200S nano hardness tester. The standard pyramid Vickers indenter is used for measurement in which the maximum load is set at 5mN and the loading time is 5s. The load-displacement curve is shown in Fig.5. Subsequently, 4 points are measured on each specimen, and the mean value is taken as the effective hardness value of the nickel-plated layer. It is obtained that the surface elastic modulus and Vickers hardness are 166.6GPa and

3483MPa, respectively. According to Tabor's research results [14], the relationship between Vickers hardness and yield stress can be expressed as

$$HV = 2.9\sigma_s \tag{2}$$

Where HV is Vickers hardness; σ_s is yield stress. According to Eq.(2), the yield stress of the nickel-plated layer is 1201MPa.

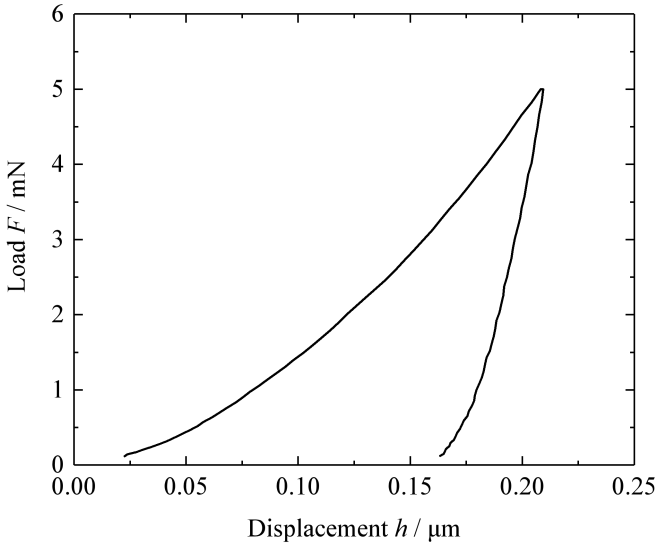

Fig.5 Load-displacement diagram of indentation test of nickel-plated layer

3. Finite element model

3.1 Model of diamond abrasive and nickel-plated layer

Although the primary diamond crystal is the octahedron, the abrasives adhered on the surface of electroplated diamond wire saw are the crushed diamond crystal. And it is found that most of the cutting edge shapes of abrasives with sawing effect are triangular pyramid by scanning the three-dimensional shapes of diamond abrasives on the surface of the diamond wire saw with a laser microscope. The measurement results of the abrasive geometry give the average angles of $\alpha_f = 66°$ for the face angle, $\alpha_r = 76°$ for the ridge angle, and $\alpha_w = 112°$ for the wedge angle [15]. To simplify the calculation of the sawing force of the diamond abrasive cutting edge, the diamond abrasive tip can be regarded as an equivalent conical tip with the average half-included angle $\psi_a = 76.903°$ [16]. Meanwhile, considering the symmetry of abrasive, a double-cone diamond abrasive model with a diameter of 10μm and an average half-included angle of 76.903° is established in this paper and the abrasive protrusion height accounts for about 1/3 of its diameter. The size of the nickel-plated layer embedded with the

diamond abrasive is much larger than the diameter of the abrasive, and its material properties are consistent with the results measured in the previous section, as shown in Table 2.

In the finite element model, the contact type between the diamond abrasive and the nickel-plated layer is set as friction contact, and the friction coefficient is 0.1 [8]. Considering the difference of material properties between diamond and nickel and the judgment basis of the abrasive shedding which is the deformation of the nickel-plated layer, the diamond abrasive is set as a rigid body in this analysis and the C3D4 linear tetrahedral element is used to mesh the model. Additionally, the mesh refinement of the nickel-plated layer around the diamond abrasive is carried out to reflect the variation of stress gradient in the finite element model, which can ensure the accuracy of finite element analysis. Based on the grid independence analysis, the finite element model of the diamond abrasive and the nickel-plated layer established in this paper is shown in Fig.6, and the specific parameters are shown in Table 2.

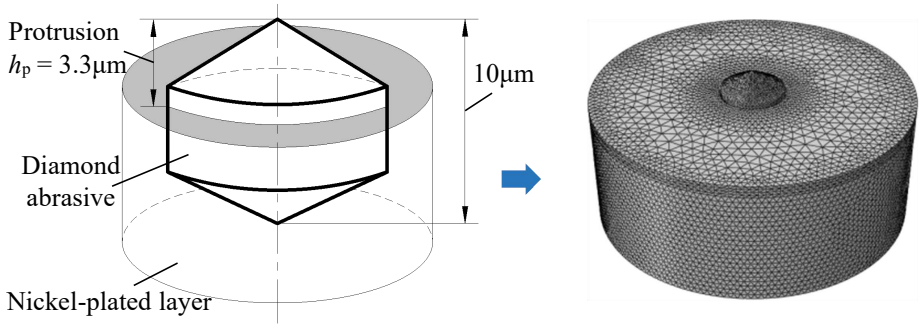

Fig.6 Finite element model of double-cone diamond abrasive embedded in nickel-plated layer

Table 2 Parameters of finite element model

Parameters	Value	
	Diamond abrasive	Nickel-plated layer
Young's modulus (GPa)	—	166.6
Poisson's ratio	—	0.3
Yield strength (MPa)	—	1201
Number of nodes	36586	152925

3.2 Setting of residual stress in finite element model

The diamond abrasive is embedded and coated on the surface of electroplated diamond wire saw by the nickel-plated layer. The residual stress in the nickel-plated layer formed on

the surface of high strength core wire by composite electroplating process is compressive stress, and it will affect the diamond abrasive retention capacity. Generally, the residual compressive stress will be decreased with the increase of thickness of the nickel-plated layer [17]. So the residual stress in the nickel-plated layer can be applied to the analysis model via the equivalent cooling method, which is achieved by pre-stress cooling of the finite element model without stress [12]. However, due to the complex geometry of diamond abrasive, the stress distribution in the finite element model is also too complex to be accurately added. Therefore, in this paper, the average stress σ_{AVG} in a certain area S_R on the surface of nickel-plated layer model without diamond abrasive is taken as the value of the surface residual stress in the finite element model, as shown in Fig.7(a) and (b). And then the residual stress is applied to the finite element model with the abrasive via the equivalent cooling method with the same temperature difference value, as shown in Fig.7(c). The stress field shown in Fig.7 indicates that the residual stress is decreased with the increase of thickness of the nickel-plated layer, and the value is higher at the geometric edge of the diamond abrasive, which is consistent with the results of relevant studies [12, 17].

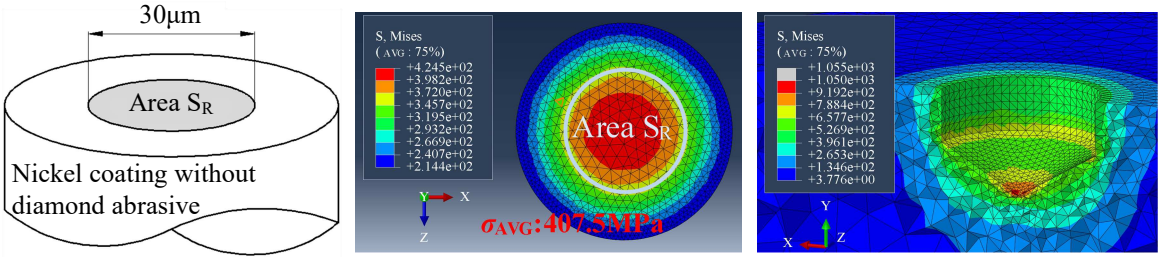

(a) Schematic diagram (b) Without diamond abrasive (c) With diamond abrasive

Fig.7 Residual stress field in nickel-plated layer

3.3 Sawing force of single diamond abrasive

In the process of diamond wire saw slicing, the sawing force F_f of the diamond abrasive cutting edge is associated with the structure of cutting edge, workpiece material, and cutting depth, and it can be decomposed into normal force F_n and tangential force F_t calculated by Eq.(3) [18]. According to the relationship between F_n and F_t, the direction of the sawing force F_f loaded to the abrasive in the finite element model can be obtained.

$$\begin{cases} F_{\mathrm{n}} = h_{\mathrm{a}}^2 H_1 \cdot \tan^2\psi_{\mathrm{a}} \left(\dfrac{\pi}{2} - \mu\cos\psi_{\mathrm{a}} \displaystyle\int_0^{\frac{\pi}{2}} \frac{\sin\varphi}{\sqrt{1-\sin^2\varphi\cos^2\psi_{\mathrm{a}}}} d\varphi \right) \\ F_{\mathrm{t}} = h_{\mathrm{a}}^2 H_1 \cdot \tan\psi_{\mathrm{a}} \left(1 + \dfrac{\mu}{\cos\psi_{\mathrm{a}}} \displaystyle\int_0^{\frac{\pi}{2}} \sqrt{1-\sin^2\varphi\cos^2\psi_{\mathrm{a}}}\, d\varphi \right) \end{cases} \tag{3}$$

Where ψ_{a} is the half-included angle of diamond abrasive; H_1 is the hardness of workpiece material; h_{a} is the cutting depth of single abrasive; μ is the friction coefficient between the diamond abrasive and the workpiece. If the sawing force loaded to the abrasive is large enough so that the deformation of the nickel-plated layer reaches a critical value, there will be an obvious gap between the nickel-plated layer and the diamond abrasive, which will make the abrasive shed, as shown in Fig.8.

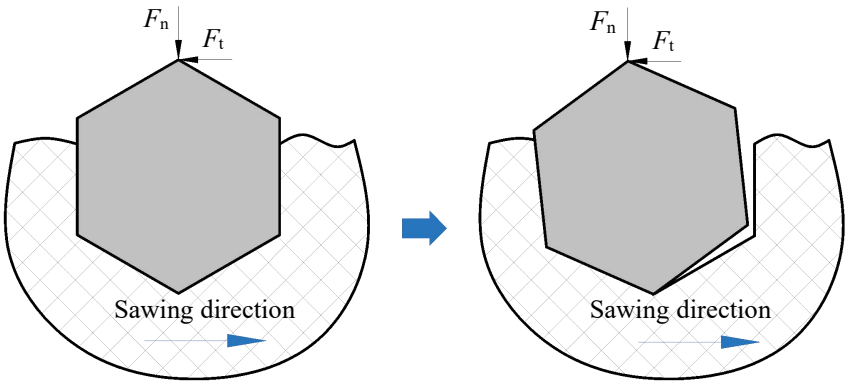

Fig.8 Sawing force of diamond abrasive

4. Results and discussions of finite element analysis

In the finite element analysis model, the stress and deformation in the nickel-plated layer are generated via applying the load corresponding to the sawing force to the diamond abrasive, as shown in Fig.9. Generally, when the plastic strain of the nickel-plated layer embedded with the diamond abrasive reaches 4%-8%, there will be an obvious gap between the abrasive and the nickel-plated layer. In this case, it can be considered that the retention effect of the nickel-plated layer has failed, and the diamond abrasive is in the critical shedding state [12]. Therefore, it is regarded as the judgment condition of abrasive shedding that the plastic strain of the nickel-plated layer is more than 8% in this paper. At this time, the sawing force applied on the abrasive is defined as the critical load of abrasive shedding F_{fmax} which is the maximum holding force of the nickel-plated layer to reflect the abrasive retention capacity. As shown in Fig.9, the maximum plastic strain caused by the sawing force

is found at the geometric edge of the extruded side of the nickel-plated layer, which is consistent with the research conclusion of Konstanty J [12].

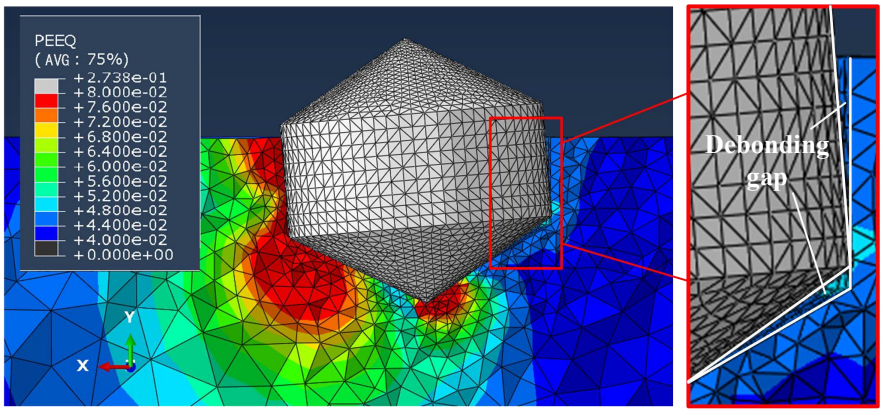

Fig.9 Critical shedding state of diamond abrasive

4.1 Influence of residual stress in nickel-plated layer on abrasive retention capacity

With the change of temperature, the stress will be produced in the nickel-plated layer. Assuming that the stress of the nickel-plated layer changes linearly with temperature, according to the principle of the equivalent cooling method, the residual compressive stress σ_{AVG} in the nickel-plated layer is modified via the adjustment of temperature difference of cooling. Then, the residual compressive stress field is applied to the finite element model of the nickel-plated layer according to this method proposed in Section 3.2. The sawing force is added to the diamond abrasive in the nickel-plated layer with a certain stress field. When the plastic strain of the nickel-plated layer reaches 8%, this sawing force is considered as the critical load of abrasive shedding. The influence of the residual compressive stress in the nickel-plated layer on the abrasive retention capacity is shown in Fig.10. With the increase of the residual compressive stress in the nickel-plated layer, the critical load of diamond abrasive shedding is decreased, which will reduce the abrasive retention capacity of the nickel-plated layer so that the abrasive is easier to shed. So the existence of residual compressive stress in the nickel-plated layer is not conducive to the abrasive retention capacity [19].

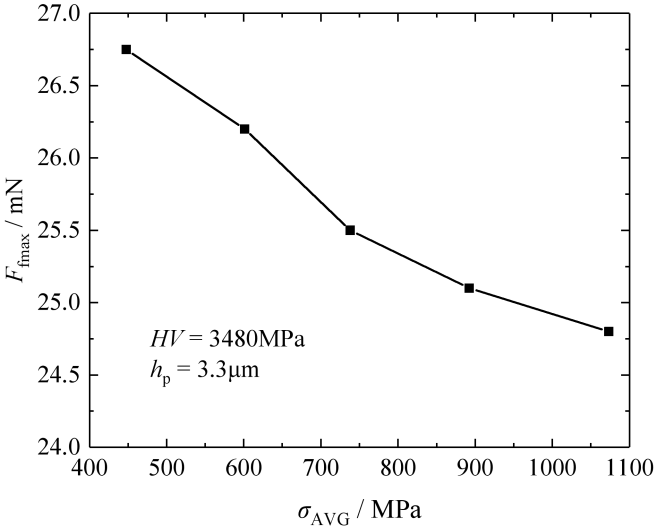

Fig.10 Influence of residual stress in nickel-plated layer on abrasive retention capacity

4.2 Influence of hardness of nickel-plated layer on abrasive retention capacity

The hardness of the nickel-plated layer is an important parameter to reflect its mechanical properties. However, hardness can not be directly set as a material parameter in ABAQUS. Therefore, the Vickers hardness is transformed into the yield stress of the material by Eq.(2) to accomplish the modification of the hardness of the nickel-plated layer material in the simulation, so as to obtain the critical loads of diamond abrasive shedding in the nickel-plated layer with different hardness values, as shown in Fig.11. The higher the hardness of the nickel-plated layer, the greater the load needed to produce plastic deformation, which will make the retention effect of the nickel-plated layer stronger so that it is more difficult for the abrasive to shed from the surface of the nickel-plated layer. The results show that when the hardness of the nickel-plated layer is increased by about 108%, the abrasive retention capacity of the nickel-plated layer is enhanced by about 23%.

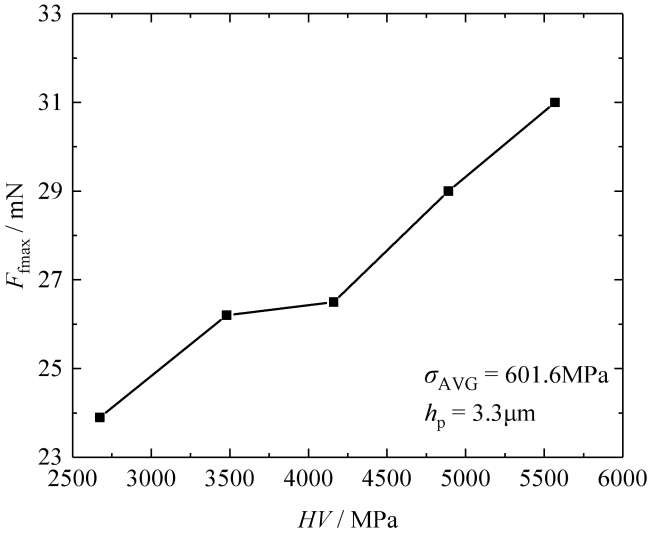

Fig.11 Influence of hardness of nickel-plated layer on abrasive retention capacity

4.3 Influence of abrasive protrusion height on abrasive retention capacity

The protrusion height of diamond abrasive is one of the important parameters that affect the sawing efficiency of the diamond wire saw. Generally, the reasonable protrusion height should be 1/3-1/2 of the diameter of diamond abrasive [20]. In addition, the abrasive protrusion height has a non-negligible influence on the abrasive retention capacity of electroplated diamond wire saw. In this paper, the protrusion height values are divided into five cases, as shown in Fig.12. The dotted line in the figure represents the upper surface of the nickel-plated layer embedded with the diamond abrasive. In the finite element analysis, the dotted line 1 (h_{p1} = 3.3μm) is taken as the initial abrasive protrusion height, and the thickness of the nickel-plated layer is gradually reduced at the interval of 0.5μm on the premise that the material properties and residual stress of the nickel-plated layer are constant.

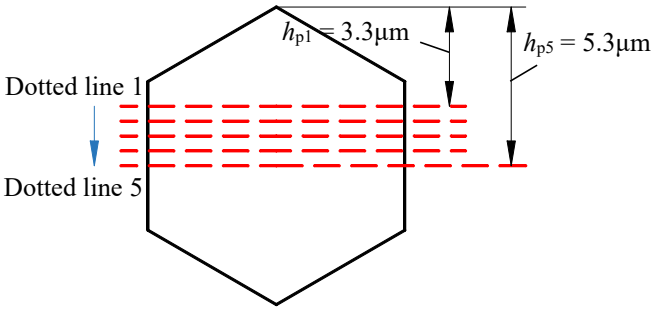

Fig.12 Schematic diagram of protrusion height of diamond abrasive

The influence of the abrasive protrusion height on the critical load of abrasive shedding is shown in Fig.13. With the increase of the protrusion height, the critical load of abrasive

shedding is decreased, which indicates that the abrasive retention capacity of the nickel-plated layer is weakened. This is because the depth of the diamond abrasive inside the nickel-plated layer is changed with the variation of the abrasive protrusion height, which affects the abrasive retention capacity of the nickel-plated layer. The results show that the abrasive retention capacity of the nickel-plated layer is decreased by about 31% when the protrusion height of double-cone diamond abrasive is increased by about 61%.

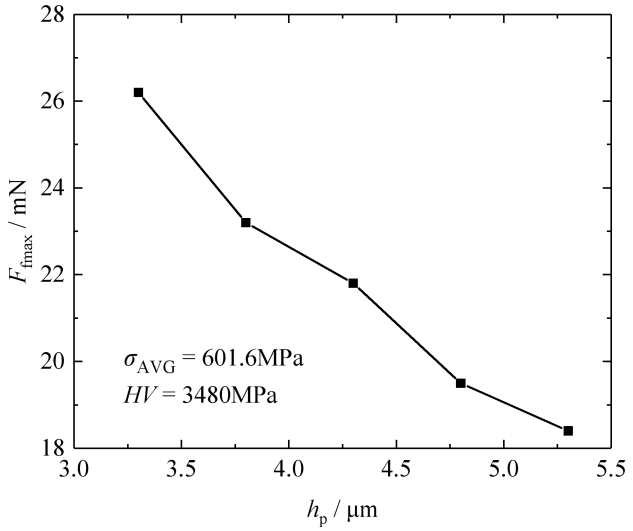

Fig.13 Influence of abrasive protrusion height on abrasive retention capacity

5. Abrasive shedding rate in sawing

5.1 Simulation procedure of abrasive shedding rate

The abrasive shedding on the surface of electroplated diamond wire saw is associated with the sawing force. In order to predict the abrasive shedding rate which can directly reflect the abrasive retention capacity of the diamond wire saw in sawing, it is necessary to establish the abrasives distribution model to determine the position of the randomly distributed abrasives, so as to calculate the cutting depth of each abrasive and then obtain the abrasive sawing force [20, 21]. As shown in Fig.14, the wire saw surface is meshed into $m \times n$ grids, where m and n are the number of grids along the circumferential direction and the axial direction respectively. The unit length of the two directions is the same to ensure that the possibility of the existence of diamond abrasive in each grid is equal, which can be expressed as

$$\frac{\pi d}{m} = \frac{l}{n} \tag{4}$$

Where d is the outer diameter of the diamond wire saw; l is the contact length between the saw wire and the workpiece in sawing.

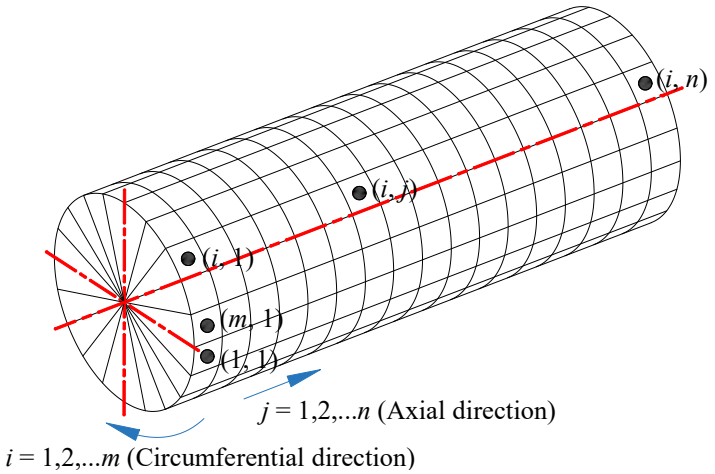

Fig.14 Mesh model of the surface of electroplated diamond wire saw

The total number of abrasives in the contact length between the saw wire and the workpiece with an abrasive density of η is

$$N = \pi\eta dl \tag{5}$$

The meshed wire can be seen as a two-dimensional zero matrix M with m rows and n columns. N non-zero numbers are randomly inserted into the matrix without repetition, and the row number i and column number j of non-zero element M_{ij} in the matrix are recorded. In the following process of defining the abrasive properties, the ith row and jth column with the non-zero numbers are calculated successively until the definition of N abrasives is completed. The position angle of abrasive is

$$\theta_{ij} = 2\pi(i - 1/2)/m \tag{6}$$

The cutting depth model of arbitrary abrasive on the wire cross-section is shown in Fig.15. In order to simplify the calculation program, the change of abrasive size is ignored in this paper. The abrasive protrusion height defined as a random one of the five height values in Section 4.3 can be expressed as

$$h_{pij} = round[(n_p - 1)rand(1)]\Delta h_p + h_{p1} \tag{7}$$

Where n_p is the selected number of the abrasive protrusion height values, n_p = 5; Δh_p is the interval of the abrasive protrusion height values, Δh_p = 0.5μm; h_{p1} is the initial abrasive protrusion height, which is 1/3 of the diameter of diamond abrasive, h_{p1} = 3.3μm.

Therefore, the cutting depth of diamond abrasive can be obtained as

$$h_{aij} = L\sin\theta_{ij} - \left(h_{pmaxj} - h_{pij}\right) \tag{8}$$

Where L is the displacement of downward movement of the wire cross section in the simulation; h_{pmaxj} is the maximum abrasive protrusion height in the jth section. If $\theta_{ij} \in [\pi, 2\pi]$ or $h_{aij} \le 0$, $h_{aij} = 0$.

Substituting Eq.(8) into Eq.(3), the sawing force of the abrasive can be calculated by

$$F_{fij} = \sqrt{F_{nij}^2 + F_{tij}^2} \tag{9}$$

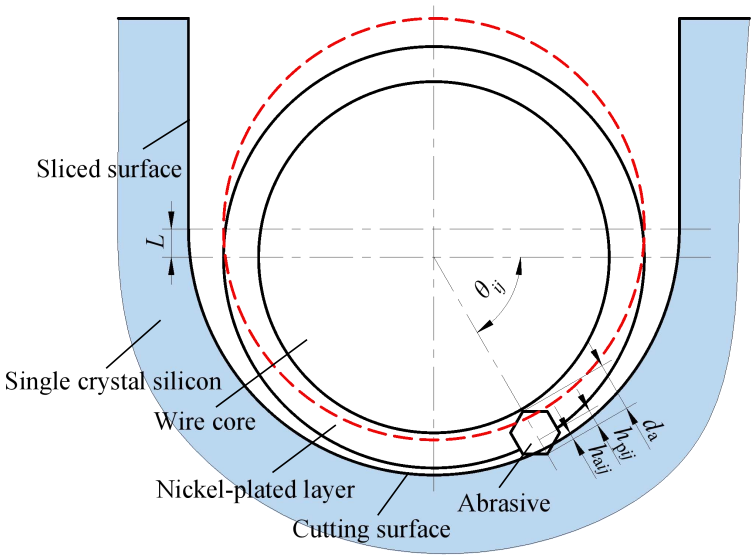

Fig.15 Cutting depth of arbitrary abrasive on wire cross-section

The simulation procedure for predicting the abrasive shedding rate shown in Fig.16 mainly includes three steps: 1) The position and protrusion height of the abrasive are generated by the input parameters including the geometric and mechanical properties of the saw wire and the workpiece as well as the sawing parameters. Meanwhile, the critical load F_{fmaxij} of abrasive shedding with the different protrusion height of the abrasive embedded in the nickel-plated layer with a certain residual compressive stress and hardness is calculated on the basis of the finite element analysis method in Section 3; 2) The normal force and tangential force of each abrasive are solved according to the displacement L. In the slicing process, it is necessary to meet the requirement that the sum of the sawing forces in the feed direction of the abrasives is equal to the normal sawing force caused by the bending of the saw wire at all times. In this paper, the abrasive shedding state is judged by the sawing force of the abrasive at the maximum bow angle θ_b in sawing. Therefore, the simulation procedure is carried out with the increase of displacement L until the sum of the normal forces on the

abrasives in the feed direction $\sum F_{nij}\sin\theta_{ij}$ is balanced with the component of the tension force in this feed direction $2T\sin\theta_b$. Based on these, the sawing force F_{fij} of each abrasive is obtained; 3) Taking the critical load of abrasive shedding as the limiting condition, it is considered that this abrasive will shed as long as the sawing force F_{fij} is greater than the critical load F_{fmaxij}. Then, the number *Sum_Shed* of abrasives that have shed can be obtained by the above judgment method to calculate the abrasive shedding rate. Due to the random distribution of the position and protrusion height of the abrasive, there will be a certain calculation deviation in the simulation procedure. Therefore, it is necessary to simulate the same set of parameters many times, and take the average value of the output results as the valid abrasive shedding rate. Furthermore, taking into account the small deflection of the wire in the contact region [22], it is assumed that this part of the diamond saw wire in contact with the workpiece in sawing will not be bent and deform as a straight line *l* in the paper, as shown in Fig.17.

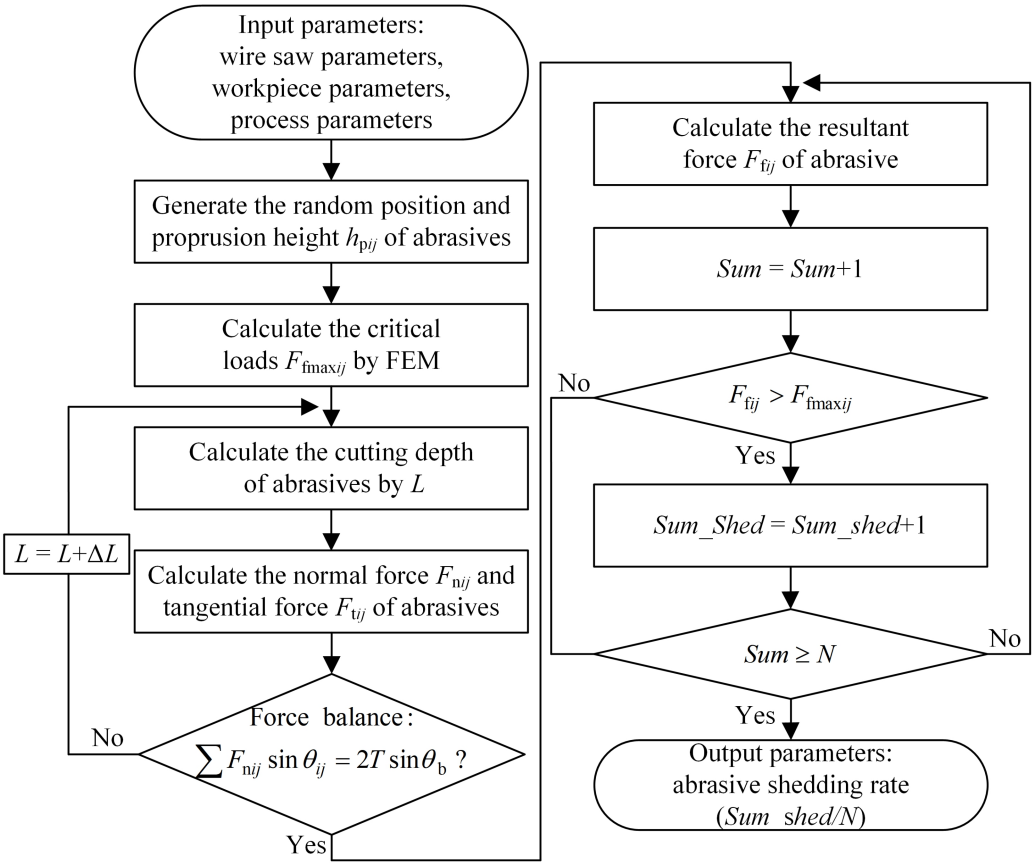

Fig.16 Simulation procedure of abrasive shedding rate

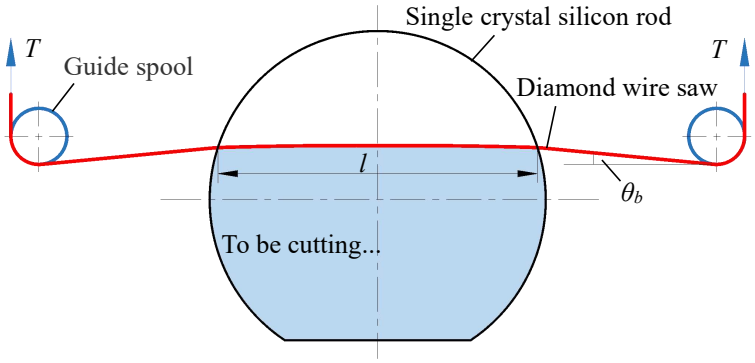

Fig.17 Schematic diagram of single crystal silicon rod sawing with diamond wire saw

5.2 Sawing experiment

In this paper, the Meyer Burger RTD6800 multi-wire sawing machine is used for this sawing experiment, as shown in Fig.18. The core wire diameter of the electroplated diamond wire saw is 65μm, and the diameter of the single crystal silicon rod is 60mm. It is generally considered that the wire saw bow should not exceed 10mm in slicing [23, 24]. Therefore, it can be obtained that the bow angle should not exceed 4° during sawing according to the structure of the Meyer Burger RTD6800. However, to improve the experiment efficiency, the feed speed is increased within a certain range, and the process parameters are shown in Table 3. After a period of sawing, the bow angle of the wire saw reaches 7.3°, as shown in Fig.19, and exposes a trend of sustained growth, which can be considered that sawing performance of the wire saw has declined significantly. The contact length between the wire and the workpiece is about 40mm in this case. At the same time, it can be seen that the surface of the wire saw after sawing has been visibly worn via the observation of the scanning electron microscope, as shown in Fig.20.

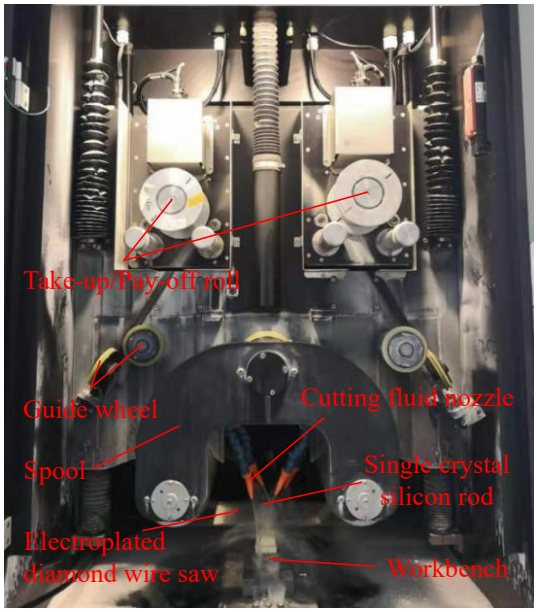

Fig.18 Structure of the Meyer Burger RTD6800 multi-wire sawing machine

Table 3 Process parameters

Parameters	Value
Wire speed (m/min)	27.3
Feed speed (mm/min)	9
Tension force (N)	10

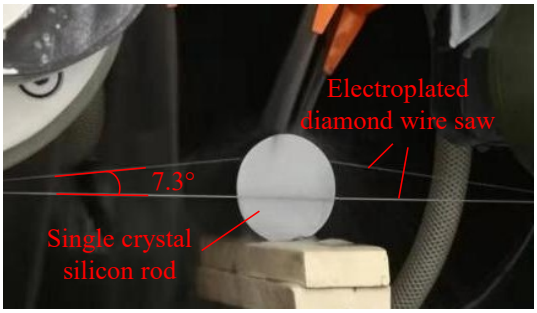

Fig.19 Sawing process

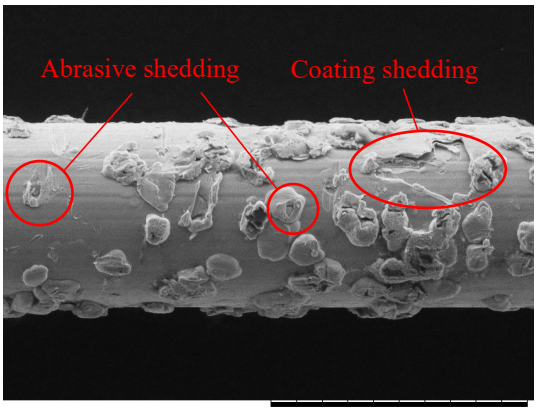

Fig.20 Morphology of electroplated diamond wire saw after experiment

KBXJ-I wire saw topography analyzer is used to analyze the abrasive shedding on the surface of electroplated diamond wire saw before and after the experiment, as shown in Fig.21. This device is based on the image detection method to measure the number and protrusion height values of abrasives. There are 10 analysis regions in this measurement, and the total length of measurement is 15mm. For this detection equipment, the cutting edge rate is calculated by the number of the abrasives whose cutting edge height is greater than 3μm. The results of measurement show that the abrasive cutting edge rate is 288.9 abrasives/mm before sawing and 204.8 abrasives/mm after sawing. So, it can be obtained that the actual abrasive shedding rate is 29.4% in the above experiment.

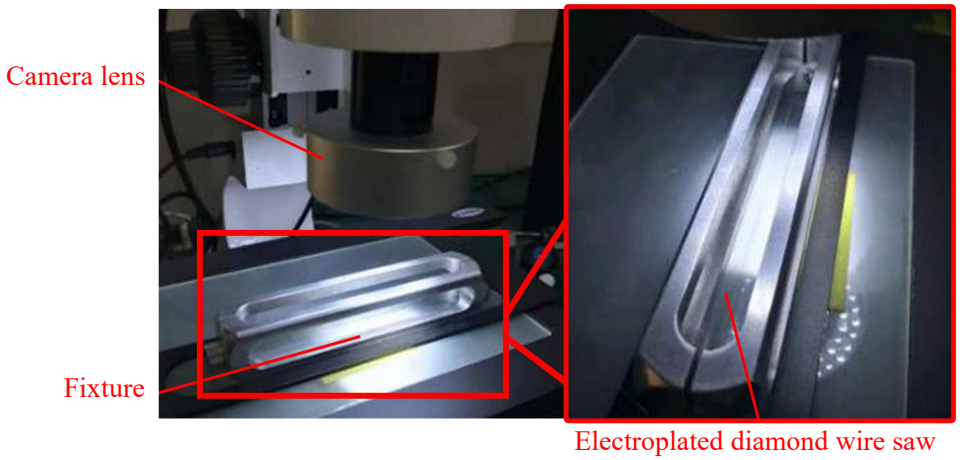

Fig.21 Analysis test of abrasive number on the surface of electroplated diamond wire saw

Furthermore, based on the simulation procedure of abrasive shedding rate described in the previous section, it can be concluded that the theoretical abrasive shedding rate of the wire saw surface after sawing is 24.6% (±1.55%) by the input parameters are shown in Table 4. The relative error between the actual abrasive shedding rate and the theoretical calculation value is about 16.3%.

Table 4 Input parameters in simulation

Parameters	Value
Wire outer diameter d (μm)	90
Density η (abrasives/mm^2)	300
Half taper angle of abrasive ψ_a (°)	76.903
Abrasive diameter d_a (μm)	10
Hardness of nickel-plated layer HV (MPa)	3483
Residual stress of nickel-plated layer σ_{AVG} (MPa)	601.6

Hardness of silicon H_1 (GPa)	10
Friction coefficient between abrasive and workpiece μ	0.2
Length of contact between wire and workpiece l (μm)	40×10^3
Tension force T (N)	10
Wire bow angle θ_b (°)	7.3

6. Conclusion

In this paper, a finite element model of the double-cone diamond abrasive embedded in the nickel-plated layer was established, and the effects of the mechanical properties of the nickel-plated layer and the abrasive protrusion height on the abrasive retention capacity on the surface of electroplated diamond wire saw were investigated. The results of finite element analysis show that the presence of the residual compressive stress in the nickel-plated layer was not conducive to the abrasive retention capacity. And the higher the hardness of the nickel-plated layer was, the more difficult it was to deform. When the hardness of the nickel-plated layer was increased by about 108%, the critical load of abrasive shedding was enhanced by about 23%. In addition, with the increase of the protrusion height, the depth of the abrasive inside the nickel-plated layer was decreased, which made the maximal holding force reduced. When the protrusion height of the diamond abrasive was increased by about 61%, the abrasive retention capacity was decreased by about 31%. On the other hand, a simulation procedure was developed to obtain the abrasive shedding rate based on the results of finite element analysis. And the slicing experiment of single crystal silicon rod was carried out to verify the theoretical value of abrasive shedding rate. The experimental results show that the finite element analysis method and the calculation program for the abrasive shedding rate proposed in this paper were reliable.

Further work is needed to take into account the change of abrasive size and the refinement of the interval of abrasive protrusion height values to Improve the accuracy of the calculation. Furthermore, the analytical method can be used to guide the development of electroplated diamond wire saw.

Author contribution

Jintao Zheng: Writing - original draft, Writing - review & editing, Investigation, Methodology.

Qian Xie: Writing - original draft, Numerical simulations. Peiqi Ge: Conceptualization, Funding acquisition, Project administration, Supervision. Jianfeng Meng: Methodology, Software and editing. Wenbo Bi: Formal analysis, Validation and Experiment.

Funding

This work was supported by the National Natural Science Foundation of China (No.51775317); and the Key Research and Development Program of Shandong Province (No.2019JZZY020209).

Availability of data and materials

All data generated or analyzed during this study are included in this published article.

Declarations

Ethics approval and consent to participate

Not applicable.

Consent for publication

The consent to submit this paper has been received explicitly from all co-authors.

Competing interests

The authors declare no competing interests.

References

[1] Hervas I, Montagne A, Van Gorp A, Bentoumi M, Thuault A, Iost A (2016) Fracture toughness of glasses and hydroxyapatite: a comparative study of 7 methods by using Vickers indenter. Ceram Int 42(11): 12740-12750. https://doi.org/10.1016/j.ceramint.2016.05.030.

[2] Gao Y, Ge P, Zhang L, Bi W (2019) Material removal and surface generation mechanisms in diamond wire sawing of silicon crystal. Mater Sci Semicond Process 103: 104642. https://doi.org/10.1016/j.mssp.2019.104642.

[3] Huang H, Wang S, Xu X (2017) Effect of wire vibration on the materials loss in sapphire slicing with the fixed diamond wire. Mater Sci Semicond Process 71: 93-101. https://doi.org/10.1016/j.mssp.2017.07.010.

[4] Li X, Gao Y, Yin Y, Wang L, Pu T (2020) Experiment and theoretical prediction for surface roughness of PV polycrystalline silicon wafer in electroplated diamond wire sawing. J Manuf Process 49: 82-93.

https://doi.org/ 10.1016/j.jmapro.2019.11.022.

[5] Li H, Gao Y, Ge P, Bi W, Zhang L (2020) Study on process parameters of fabrication fine diameter electroplated diamond wire for slicing crystalline silicon solar cell. Int J Adv Manuf Technol 106: 3153-3175. https://doi.org/10.1007/s00170-019-04860-2.

[6] Scott PM, Nicholas M, Dewar B (1975) The wetting and bonding of diamonds by copper-base binary alloys. J Mater Sci 10: 1833-1840. https://doi.org/10.1007/BF00754470.

[7] Levin E, Gutmanas EY (1990) Solid-state bonding of diamond to Nichrome and Co-20wt% W alloys. J Mater Sci Lett 9: 726-730. https://doi.org/10.1007/BF00721815.

[8] Romanski A, Lachowski J, Konstanty J (2006) Diamond retention capacity: Evaluation of stress field generated in a matrix by a diamond crystal. Ind Diam Rev 66: 43-45. https://www.researchgate.net/publication/275956460.

[9] Zhao X, Duan L, Chikhotkin VF, Weng H (2015) Summary on holding force of metallic matrix to diamond. Diam Abras Eng 35: 41-46, 50. https://doi.org/10.13394/j.cnki.jgszz.2015.6.0009. (in Chinese)

[10] Webb SW (1999) Diamond retention in sintered cobalt bonds for stone cutting and drilling. Diam Relat Mater 8: 2043-2052. https://doi.org/10.1016/S0925-9635(99)00167-3.

[11] Xu J, Sheikh AH, Xu C (2017) 3-D Finite element modelling of diamond pull-out failure in impregnated diamond bits. Diam Relat Mater 71: 1-12. https://doi.org/10.1016/j.diamond.2016.11.006.

[12] Konstanty J, Romanski A (2014) Numerical analysis of diamond retention in cobalt and a copper-base alloy. Archives Metall Mater 59: 1457-1462. https://doi.org/10.2478/amm-2014-0247.

[13] Noyan IC, Cohen JB (1987) Residual stress-measurement by diffraction and interpretation. Springer-Verlag Inc, New York.

[14] Tekkaya, Erman A (2001) Improved relationship between Vickers hardness and yield stress for cold formed materials. Steel Res 72: 304-310. https://doi.org/10.1002/srin.200100122.

[15] Mahmoud T, Tamaki J, Yan J (2003) Three-dimensional shape modeling of diamond abrasive grains measured by a scanning laser microscope. Key Eng Mater 238-239: 131-136. https://doi.org/10.4028/www.scientific.net/kem.238-239.131.

[16] Ge M, Wang P, Bi W, Ge P (2021) Fabrication of thin resin-bonded diamond wire and its application to ductile-mode wire sawing of mono-crystalline silicon. Mater Sci Semicond Process 126: 105665. https://doi.org/10.1016/j.mssp.2021.105665.

[17] Hadian SE, Gabe DR (1999) Residual stresses in electrodeposits of nickel and nickel-iron alloys. Surf Coat Technol 122: 118-135. https://doi.org/10.1016/S0257-8972(99)00328-X.

[18] Wang P, Ge P, Gao Y, Bi W (2017) Prediction of sawing force for single-crystal silicon carbide with fixed abrasive diamond wire saw. Mater Sci Semicond Process 63: 25-32. https://doi.org/10.1016/j.mssp.2017.01.014.

[19] Chen J, Mu D, Liao X, Huang G, Huang H, Xu X, et al (2018) Interfacial microstructure and mechanical properties of synthetic diamond brazed by Ni-Cr-P filler alloy. Int J Refract Metals Hard Mater 74: 52-60. https://doi.org/10.1016/j.ijrmhm.2018.03.005.

[20] Liu T, Ge P, Gao Y, Bi W (2017) Depth of cut for single abrasive and cutting force in resin bonded diamond wire sawing. Int J Adv Manuf Technol 88: 1763-1773. https://doi.org/10.1007/s00170-016-8896-6.

[21] Chung C, Tsay GD, Tsai MH (2014) Distribution of diamond grains in fixed abrasive wire sawing process. Int J Adv Manuf Technol 73(9-12):1485-1494. https://doi.org/10.1007/s00170-014-5782-y.

[22] Lin Z, Huang H, Xu X (2019) Experimental and simulational investigation of wire bow deflection in single wire saw. Int J Adv Manuf Technol 101: 687–695. https://doi.org/10.1007/s00170-018-2919-4.

[23] Zhu L, Kao I (2005) Galerkin-based modal analysis on the vibration of wire-slurry system in wafer slicing using a wiresaw. J Sound Vib 283: 589-620. https://doi.org/10.1016/j.jsv.2004.04.018.

[24] Meißner D, Schoenfelder S, Hurka B, Zeh J, Sunder K, Koepge R, et al (2014) Loss of wire tension in the wire web during the slurry based multi wire sawing process. Sol Energy Mater Sol Cells 120: 346-355. https://doi.org/10.1016/j.solmat.2013.05.047.

Figures

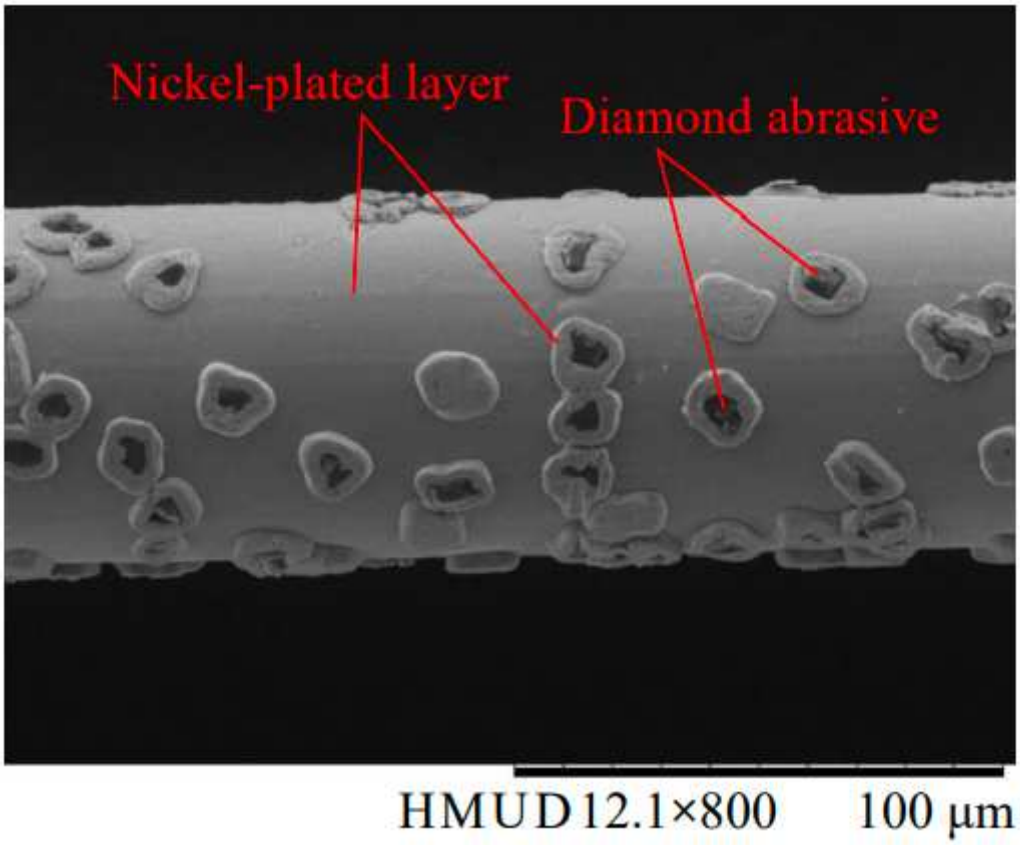

Figure 1

Please see the Manuscript PDF file for the complete figure caption

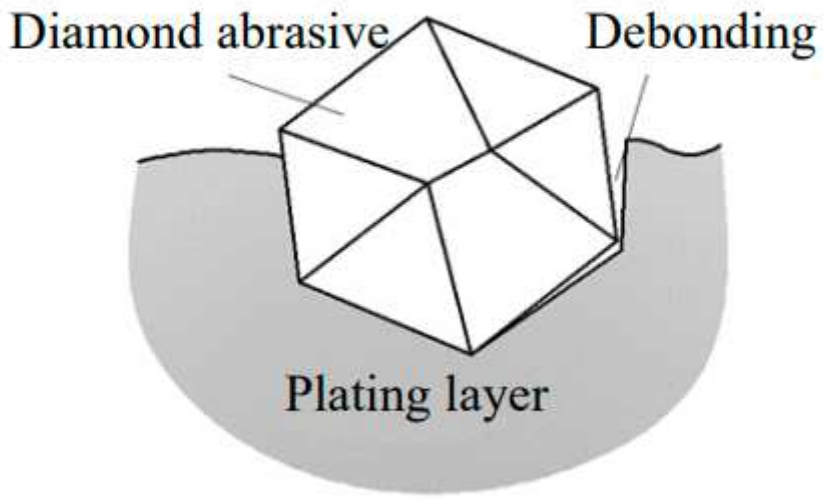

Figure 2

Please see the Manuscript PDF file for the complete figure caption

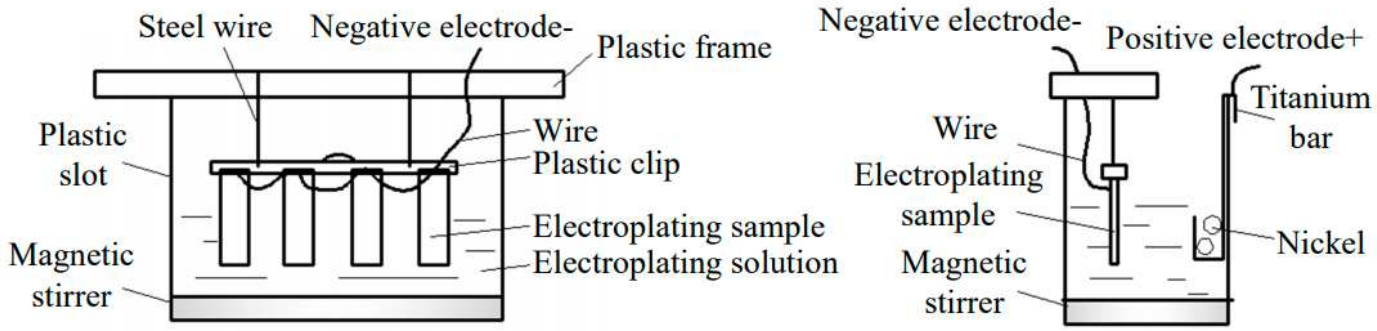

Figure 3

Please see the Manuscript PDF file for the complete figure caption

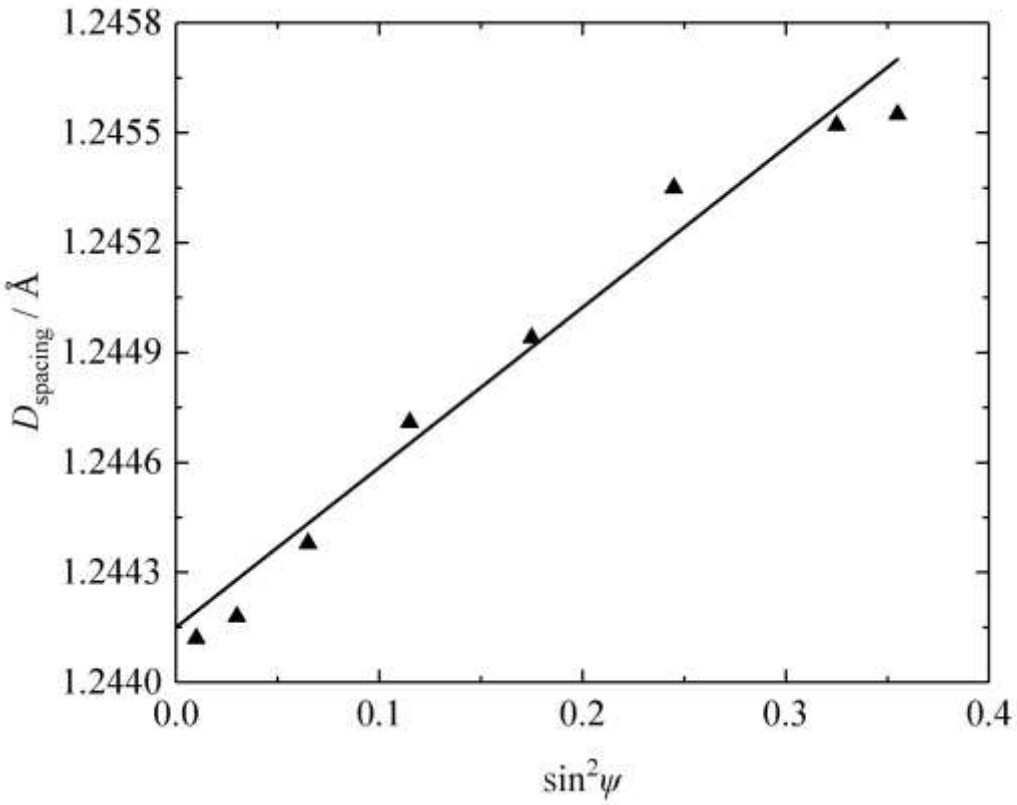

Figure 4

Please see the Manuscript PDF file for the complete figure caption

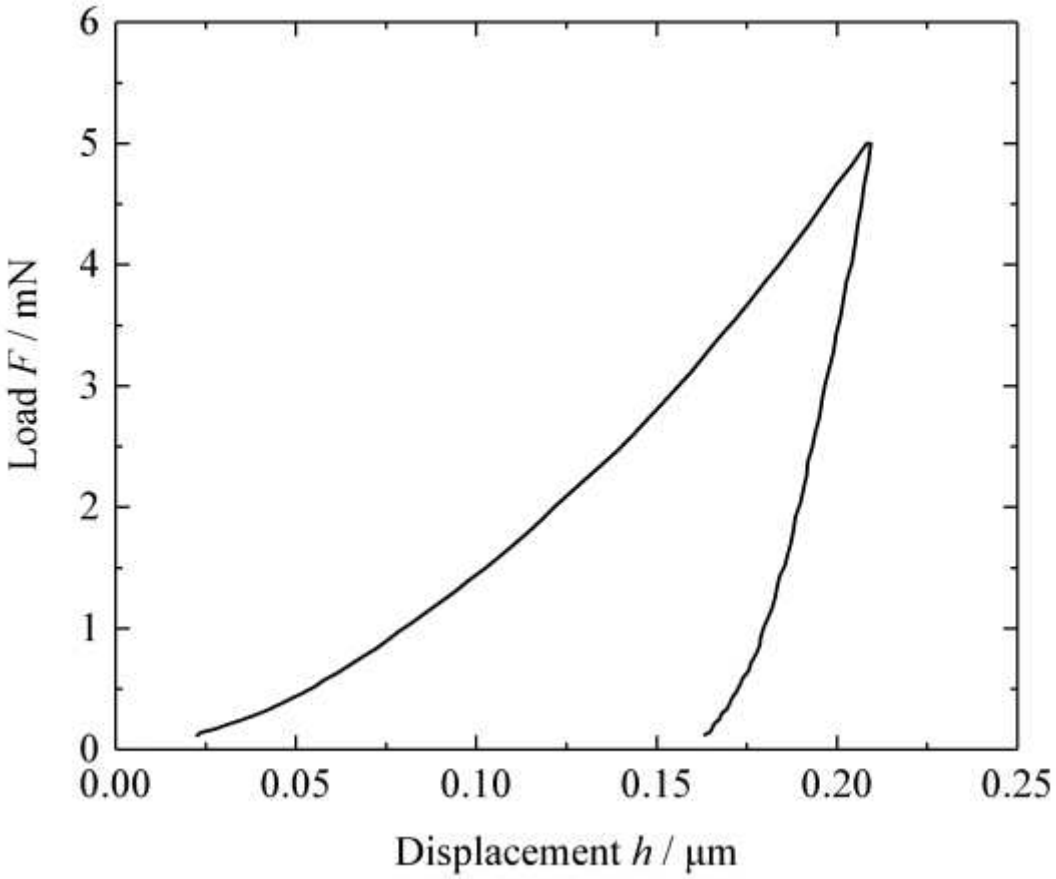

Figure 5

Please see the Manuscript PDF file for the complete figure caption

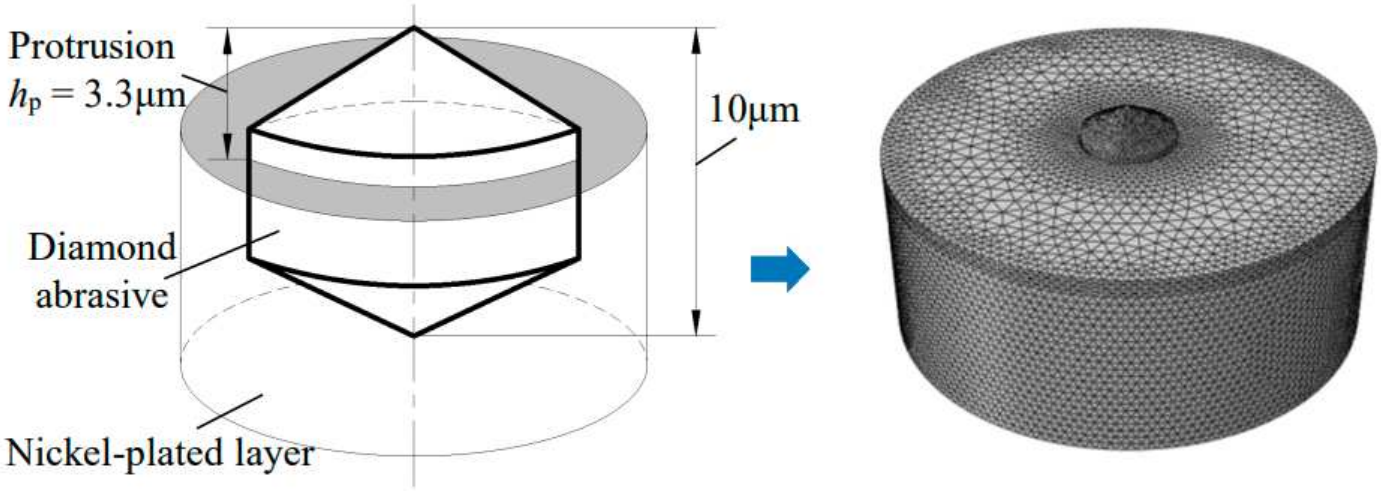

Figure 6

Please see the Manuscript PDF file for the complete figure caption

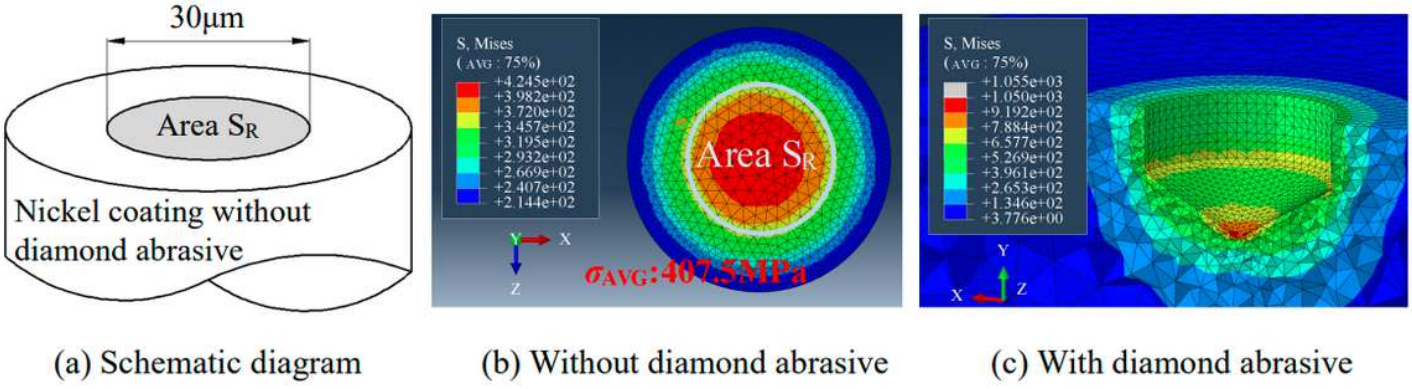

(a) Schematic diagram (b) Without diamond abrasive (c) With diamond abrasive

Figure 7

Please see the Manuscript PDF file for the complete figure caption

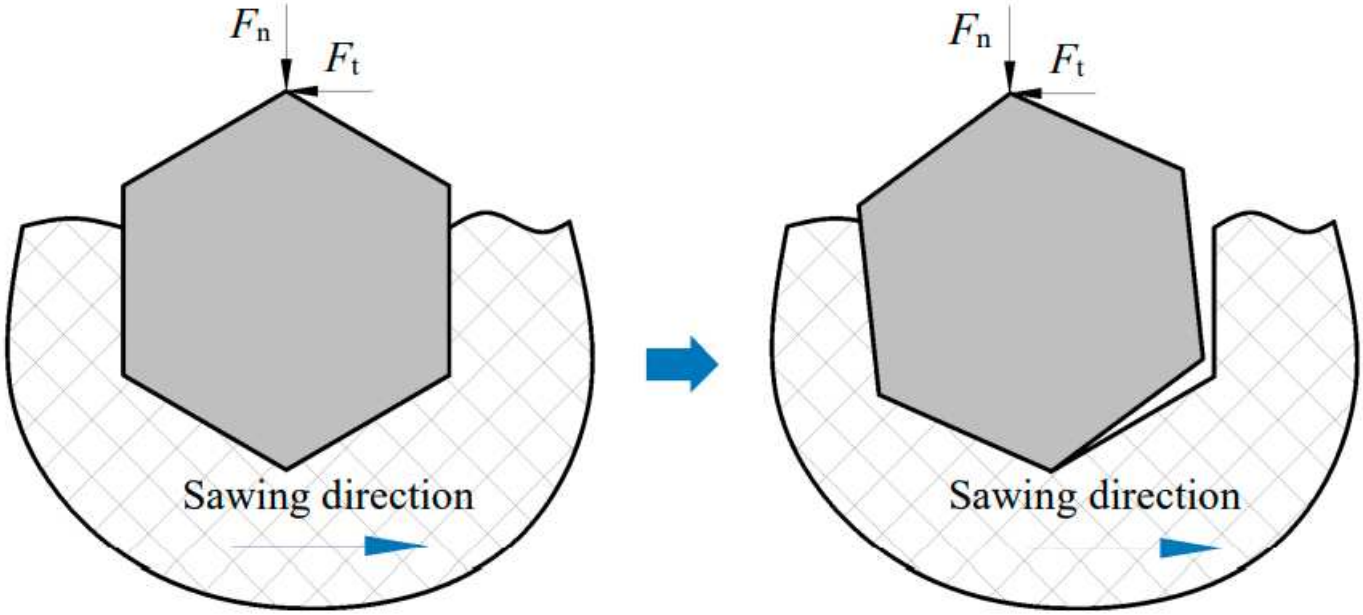

Figure 8

Please see the Manuscript PDF file for the complete figure caption

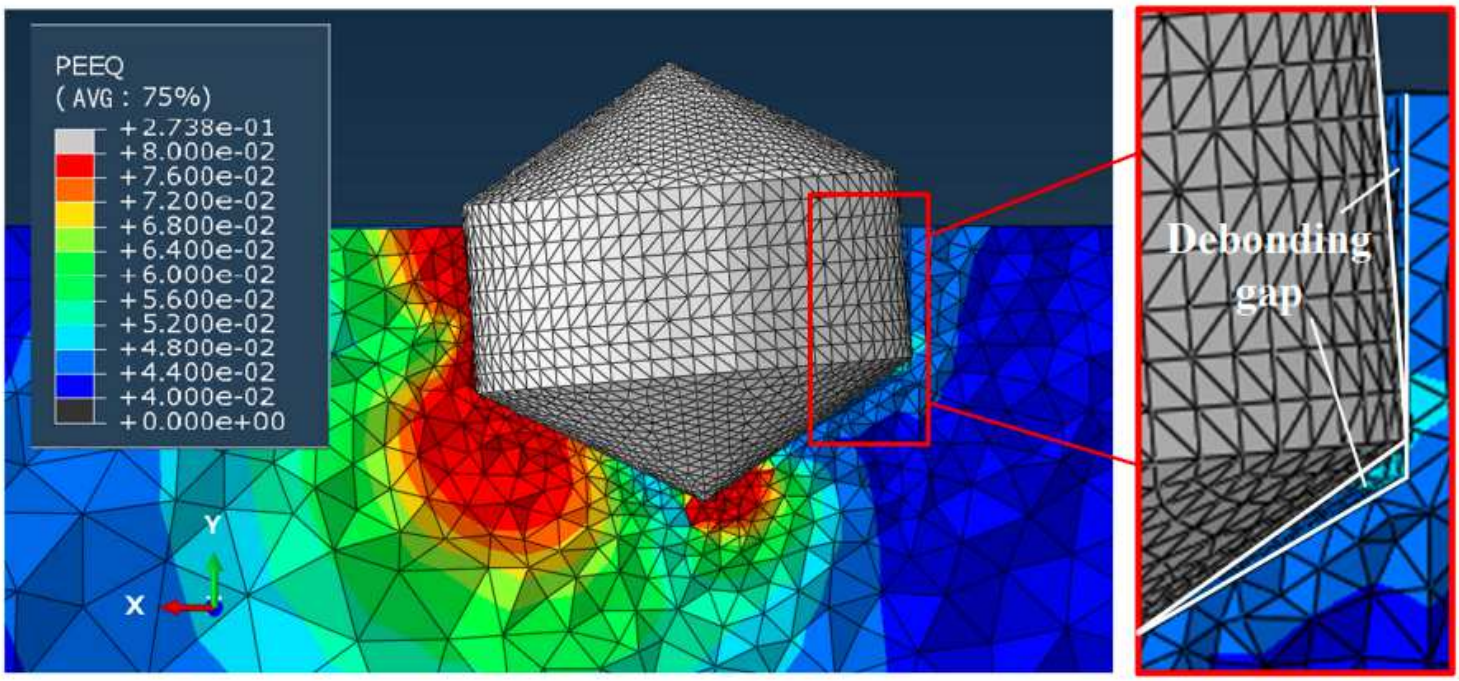

Figure 9

Please see the Manuscript PDF file for the complete figure caption

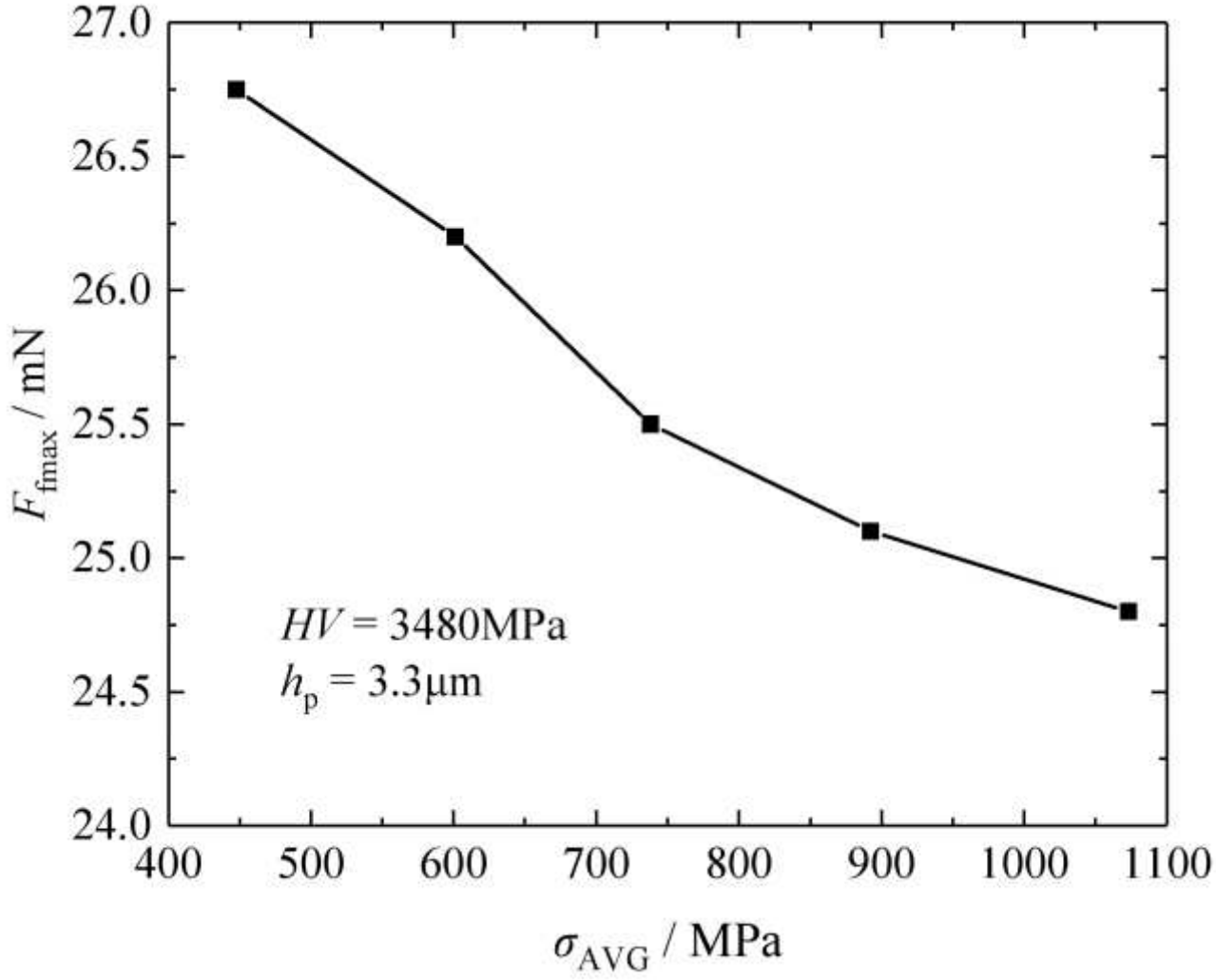

Figure 10

Please see the Manuscript PDF file for the complete figure caption

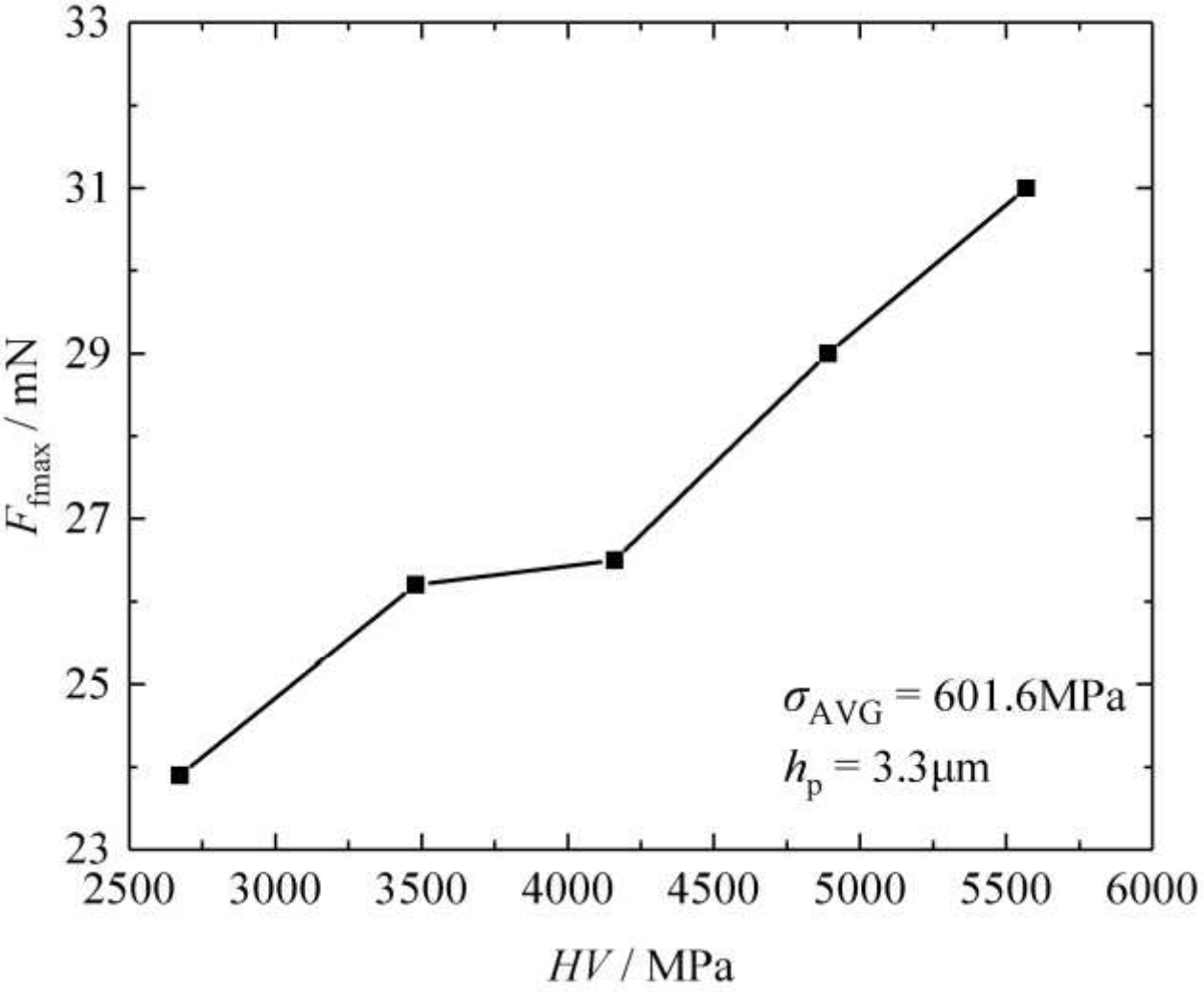

Figure 11

Please see the Manuscript PDF file for the complete figure caption

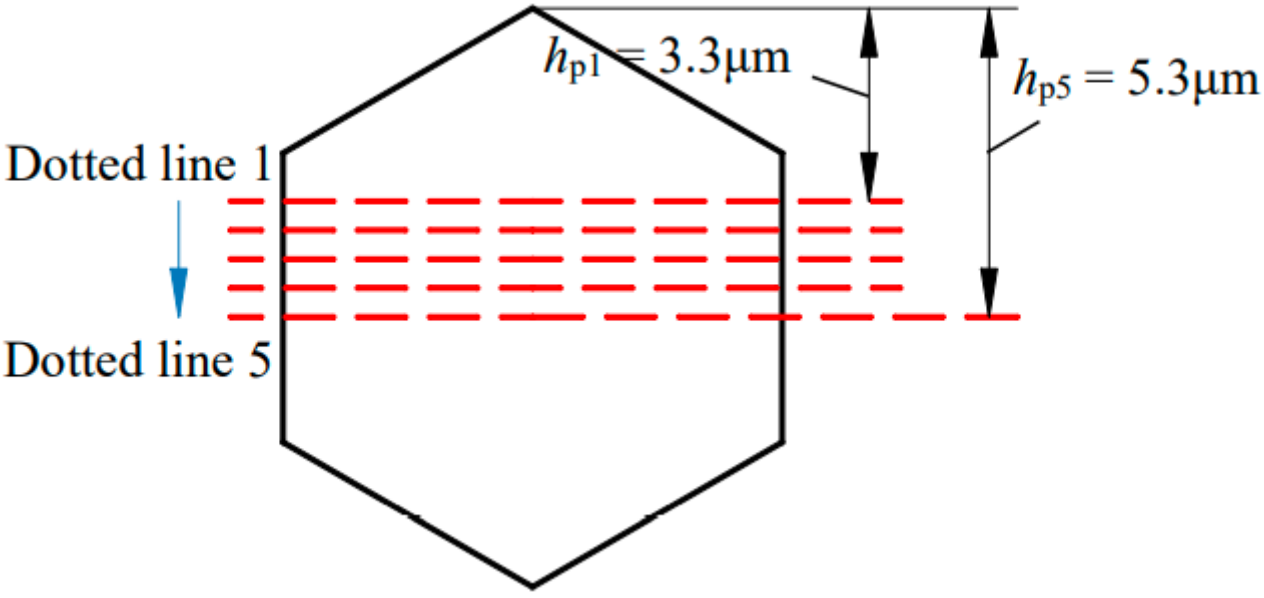

Figure 12

Please see the Manuscript PDF file for the complete figure caption

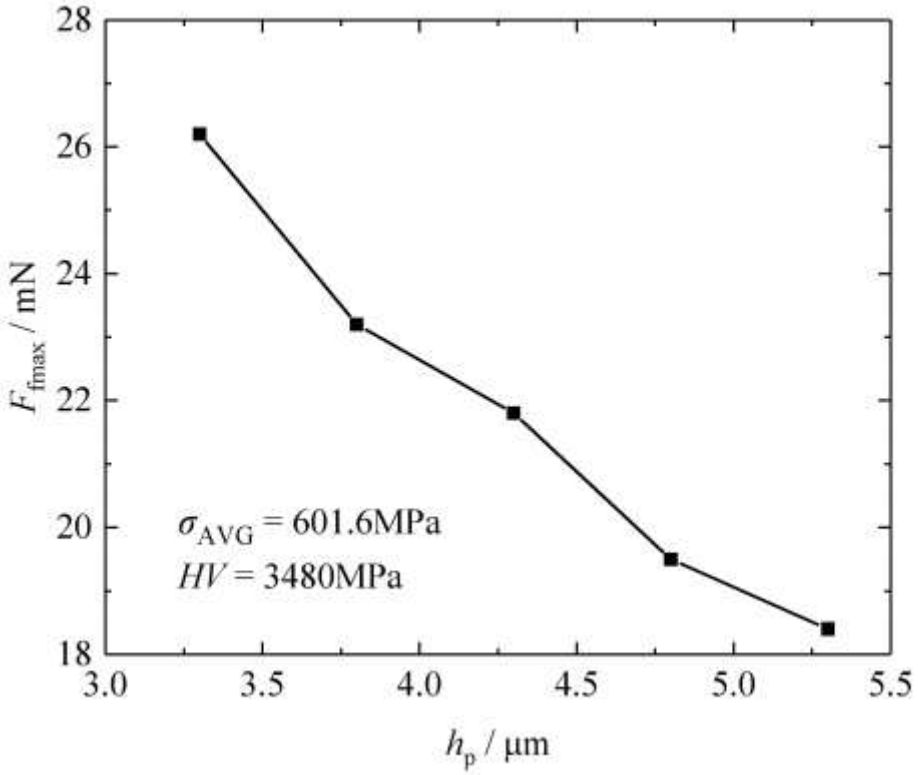

Figure 13

Please see the Manuscript PDF file for the complete figure caption

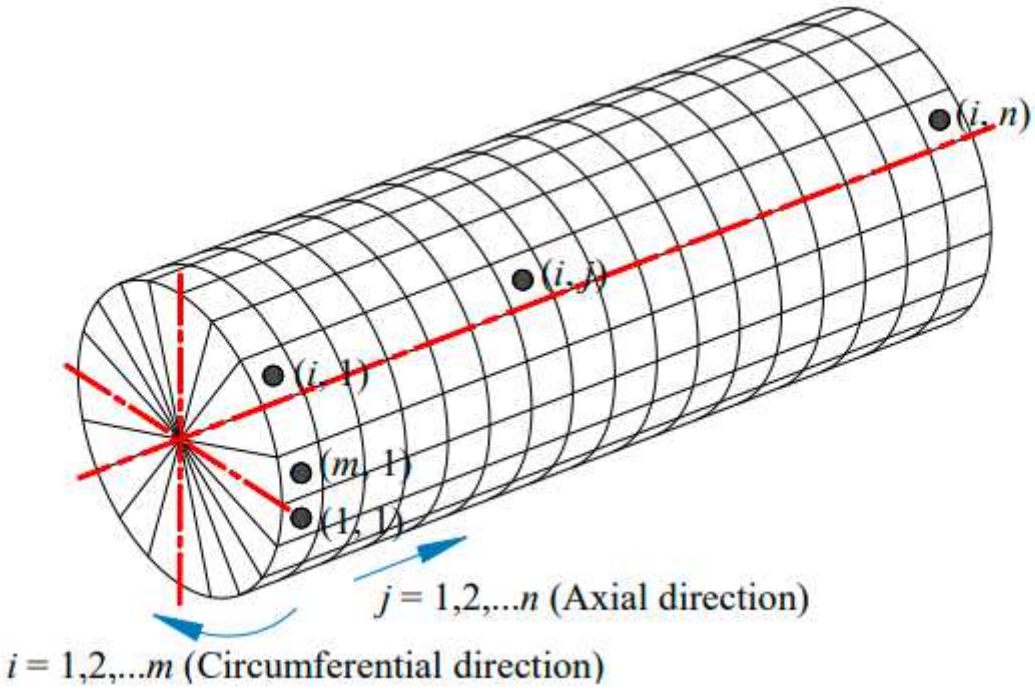

Figure 14

Please see the Manuscript PDF file for the complete figure caption

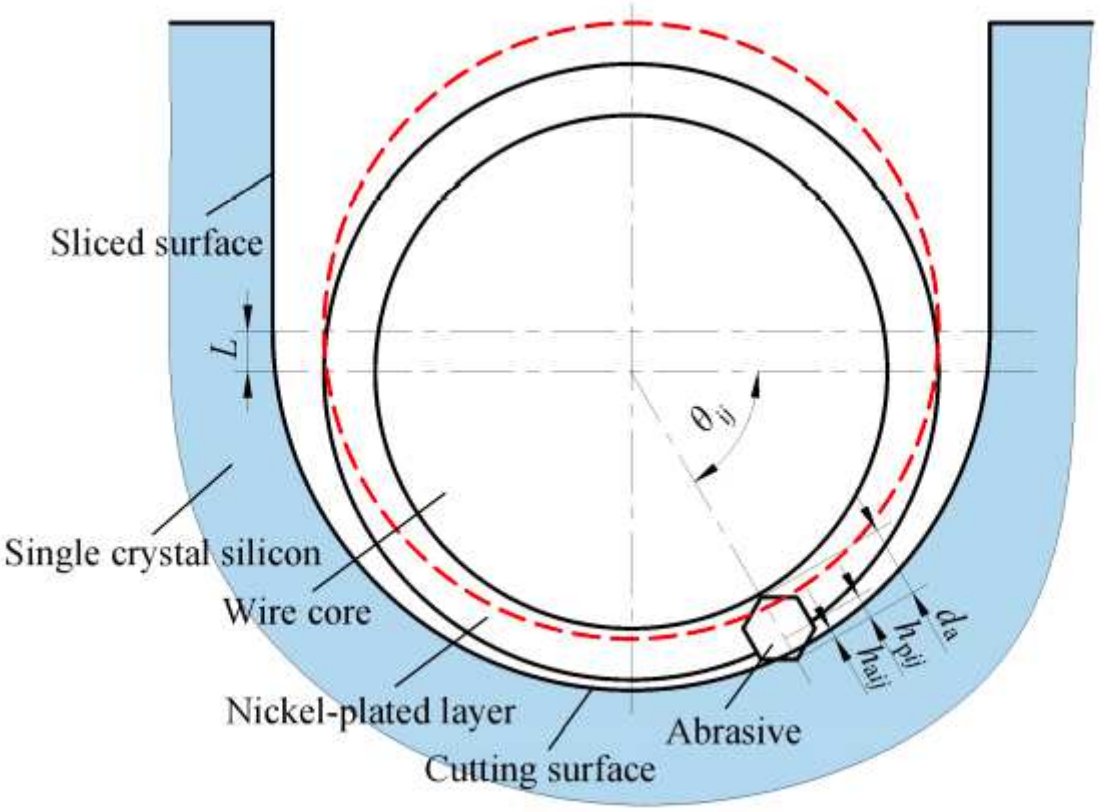

Figure 15

Please see the Manuscript PDF file for the complete figure caption

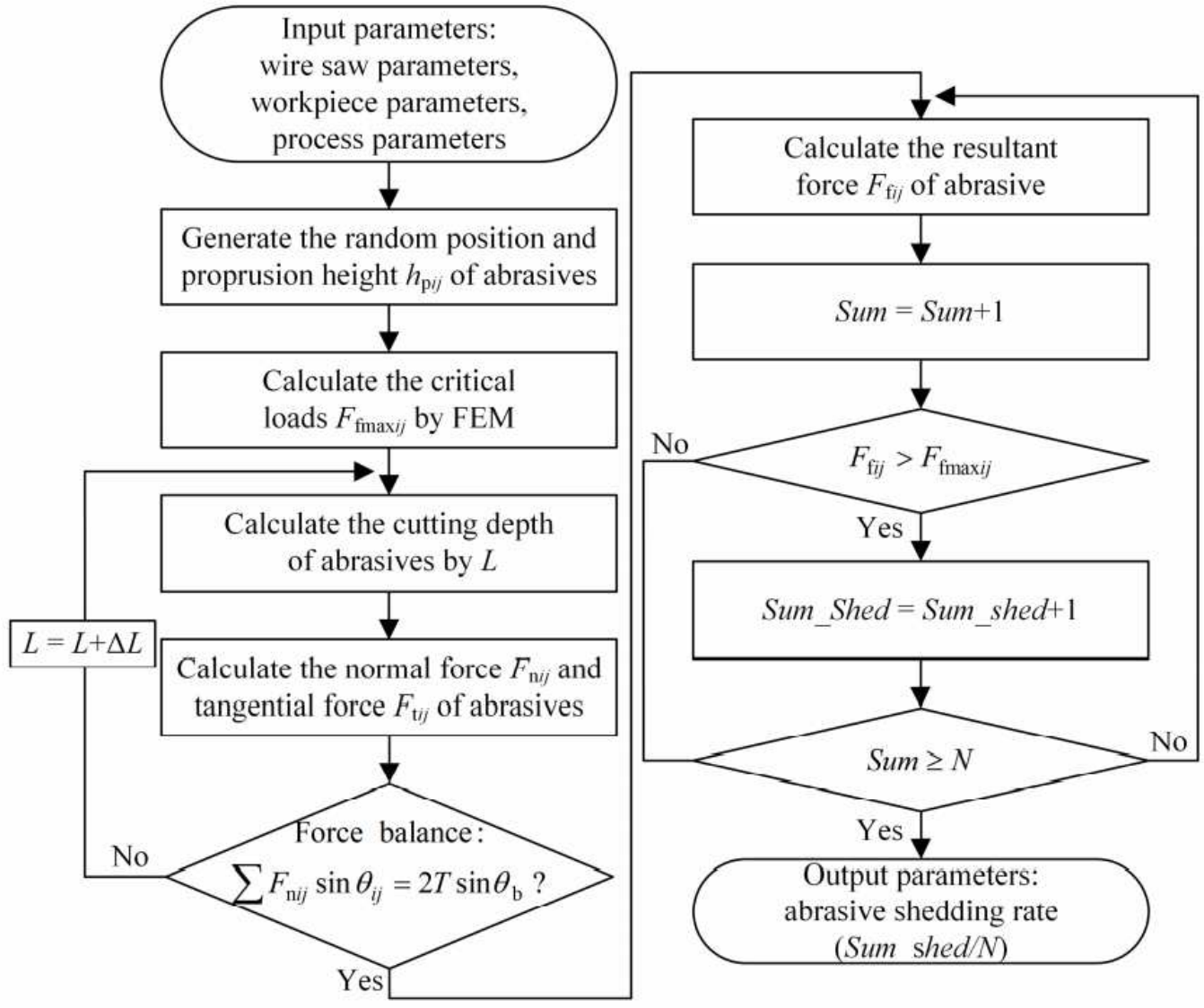

Figure 16

Please see the Manuscript PDF file for the complete figure caption

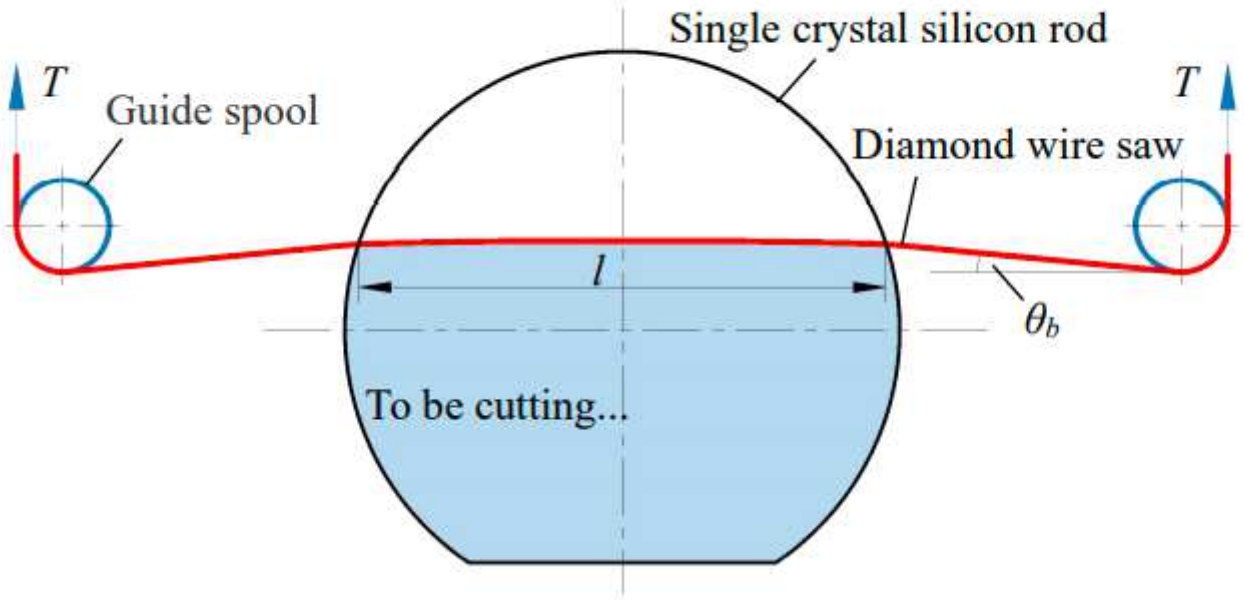

Figure 17

Please see the Manuscript PDF file for the complete figure caption

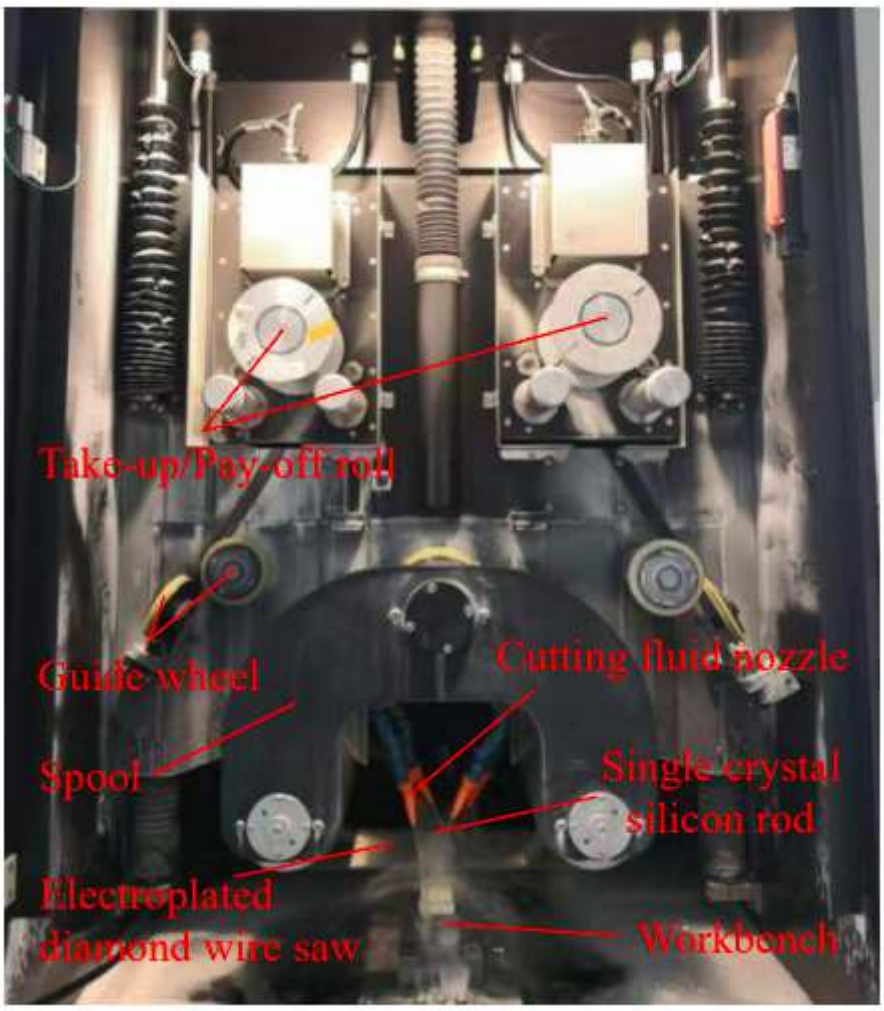

Figure 18

Please see the Manuscript PDF file for the complete figure caption

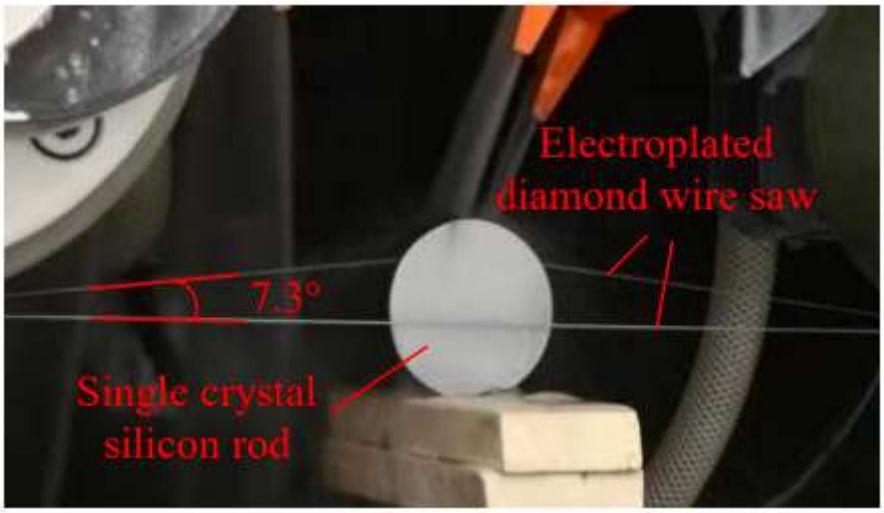

Figure 19

Please see the Manuscript PDF file for the complete figure caption

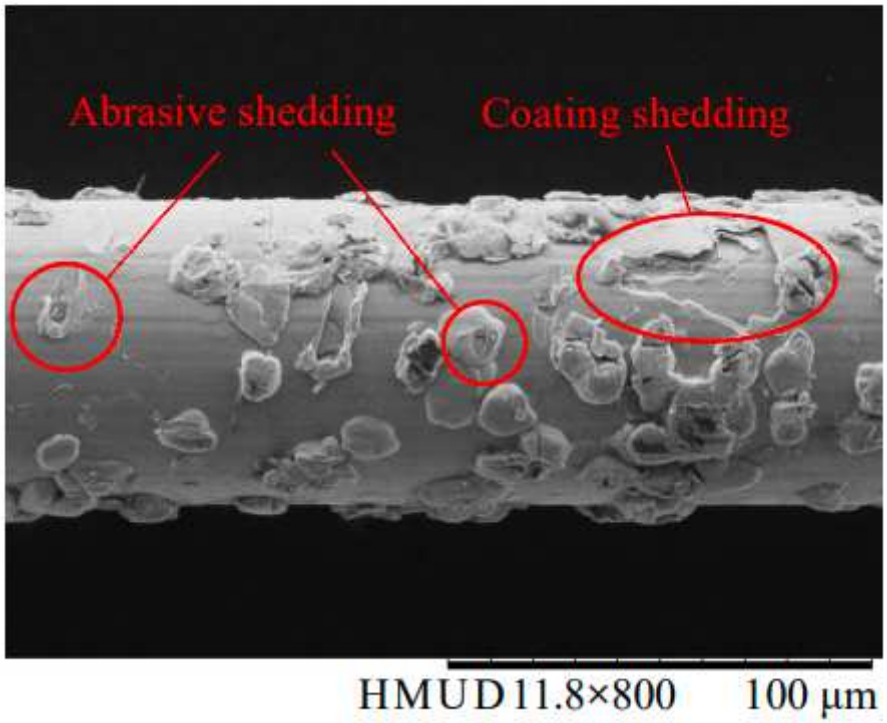

Figure 20

Please see the Manuscript PDF file for the complete figure caption

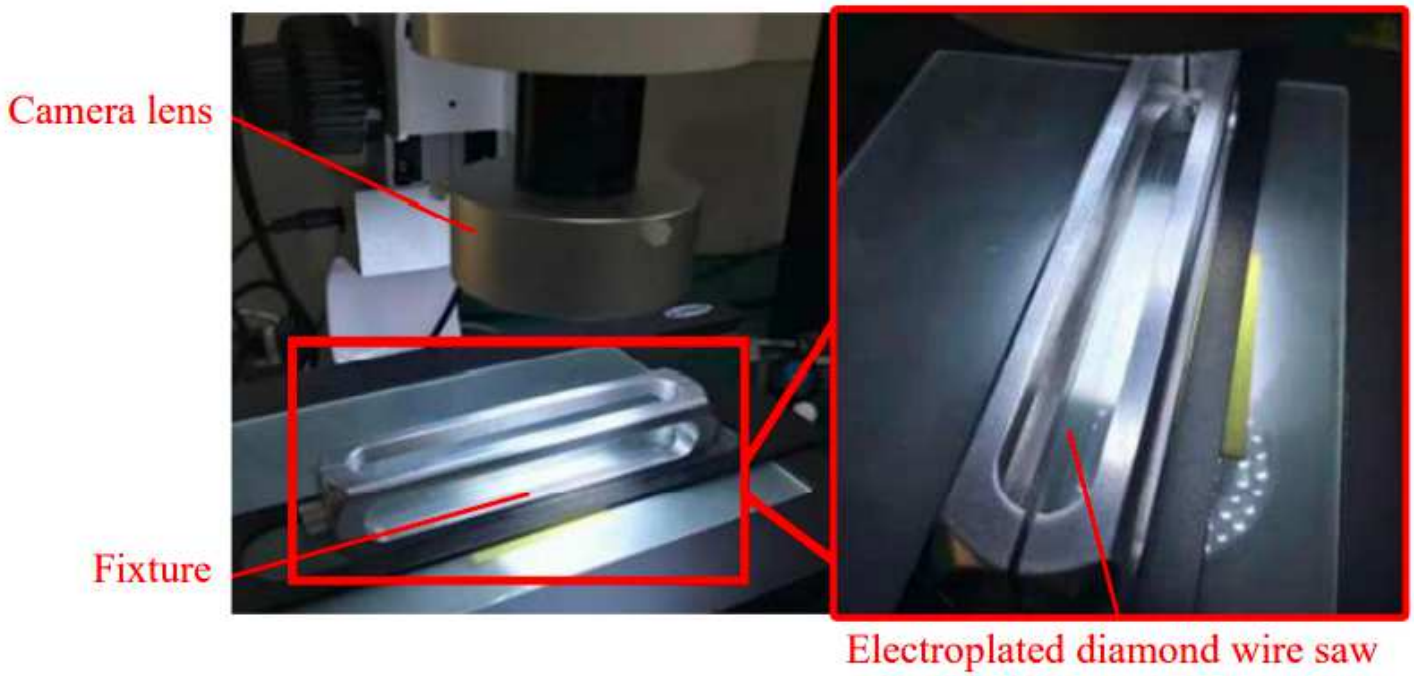

Figure 21

Please see the Manuscript PDF file for the complete figure caption